Renewable and eco-friendly ZnO immobilized onto dead sea sponge floating materials with dual practical aspects for enhanced photocatalysis and disinfection applications

Muhammad Ali Bhatti, Khalida Faryal Almani, Aqeel Ahmed Shah, Aneela Tahira, Iftikhar Ahmed Chana, Umair Aftab, Mazhar Hussain Ibupoto, Abdul Nabi Mirjat, Amal Aboelmaaref, Ayman Nafady, et al.

Renewable and eco-friendly ZnO immobilized onto Dead Sea Sponge floating materials with dual practical aspects for enhanced photocatalysis and disinfection applications

Muhammad Ali Bhatti[a], Khalida Faryal Almani[a], Aqeel Ahmed Shah[g], Aneela Tahira[b], Iftkhar Ahmed Chana[g], Umair Aftab[c], Mazhar Hussain Ibupoto[e], Abdul Nabi Mirjat[f], Amal Aboelmaare[i], AymanNafady[h], Brigitte Vigolo[d], Zafar Hussain Ibupoto[b*]

[a]Institute of Environmental Sciences, University of Sindh Jamshoro, 76080, Sindh Pakistan

[b]Dr. M.A Kazi Institute of Chemistry University of Sindh Jamshoro, 76080, Sindh Pakistan

[c]Mehran University of Engineering and Technology, 7680 Jamshoro, Sindh Pakistan

[d]Université de Lorraine, CNRS, IJL, F-54000 Nancy, France

[e]Department of Zoology, Shah Abdul Latif University Khairpur Mirs

[f]Institute of Microbiology, University of Sindh Jamshoro, 76080, Sindh Pakistan

[g]Department of Metallurgy, NED university of Engineering and Technology, Karachi Pakistan

[h]Department of Chemistry, College of Science, King Saud University, Riyadh 11451, Saudi Arabia

[i]Department of Chemistry, Faculty of Science, Helwan University, Ain Helwan, Egypt

*__Corresponding authors__ : Zafar Hussain Ibupoto& Aneela Tahira

Email: zaffar.ibhupoto@usindh.edu.pk; aneelatahira80@gmail.com

Abstract

In this study, we have investigated the role of natural Dead Sea Sponge (DSS, Porifera) as a three-dimensional (3D) porous host substrate for the immobilization of nanostructured ZnO material towards the development of ZnO based floating photocatalysts for efficient removal of methylene blue (MB) dye under the illumination of sunlight. After photodegradation, the treated water after dye degradation contains several pathogens, different disinfectants or chemical reagents are essentially used. This is not the case for DSS as it can naturally kill any pathogens during the wastewater treatment process. To explore these functions, ZnO nanosheets were incorporated onto DSS via hydrothermal protocol and the as prepared ZnO/DSS hybrid material exhibited approximately~100% degradation efficiency for the removal of MB. Importantly, the degradation kinetics associated with the fabricated ZnO/DSS was remarkably accelerated as evidenced by the high values of degradation reaction rate constants (3.35×10^{-2} min^{-1}). The outperformance of ZnO/DSS could be attributed to the adsorption caused by its 3D porous structure together with the high rapid oxidation of MB. Furthermore, the high charge separation of electron-hole pairs, natural porosity, and abundant catalytic sites offered by the hybrid ZnO/DSS floating photocatalyst in achieving approximately ~100% degradation efficiency for MB. Finally, the excellent reusability results confirm the feasibility of using natural ZnO/DSS-based photocatalyst for practical solution of wastewater treatment and other environmental problems.

Keywords: Dead Sea Sponge, ZnO, Methylene blue, Photocatalyst, Photodegradation

1. Introduction

The everyday activities of industries and households release an enormous amount of wastewater containing high levels of toxic organic compounds that ultimately cause deterioration of our environment. Among the toxic organic compounds, dyes are heavily carried by the wastewater coming from printing, food and textile industries [1]. It has been evident that approximately 30-40% wastage of dyes from textile industries is thrown as effluents into the aqueous system without pre-treatment, thereby causing several diseases including cancer [2]. For this purpose, several approaches have been used to remove dyes from the wastewater such as chemical precipitation, sorption, membrane filtration, oxidation/reduction, ion exchange, coagulation, solvent extraction, and photocatalysis [3, 4]. The use of photocatalysis is intensively employed to transform the organic dyes into carbon dioxide and water through mineralization [5].

The pre-requirement of potential photocatalysis is the design of extremely photosensitive material, therefore various semiconducting metal-oxide materials, including titanium dioxide (TiO_2) [6], zinc oxide (ZnO) [7] and cupric oxide (CuO) [8], have been investigated. ZnO, in particular, has shown significant photocatalytic activity because of its high photosensitivity [9-13]. However, the issue of agglomeration of ZnO particles, commonly observed during the degradation process in solution, impairs the photo-reactivity towards the dye degradation [14]. The fast recombination rate of electron- hole pairs is also strongly limiting the photocatalytic activity of ZnO during the illumination of light due to its wide band gap of 3.37 eV. The direct use of ZnO particles as a slurry is a general approach for the degradation of organic dyes in wastewater. However, the recovery of these particles from solution after the degradation process is still a very challenging task causing the wastage of particles as a result of post treatment processes [15, 16]. Importantly, the ZnO particles could be seen even in treated wastewater and that could be toxic to our health [17]. For overcoming all these issues, several photocatalysts have been immobilized on various supports or polymers, therefore the fabrication of semiconducting materials on supporting substrates becomes a preferential methodology[18, 19, 20]. In particular, the use of polymers as a support has been markedly implemented in the field of photocatalysis for handling environmental tasks owing to the simple reusability and low cost [21-24]. Among these polymers, polydimethylsiloxane (PDMS) is widely used in diverse fields such as biomedical and material sciences because of its outstanding physical and chemical characteristics [25]. PDMS possesses also excellent properties such as high elasticity,

nontoxicity, hydrophobicity, inertness towards fire and excellent flexibility [26, 27]. The use of PDMS immobilized with semiconducting materials have been investigated either for physical adsorption or photocatalysis [24, 28, 29]. In a recent study, porous 3D ZnO/PDMS sponge has been synthesized by sugar templating method to degrade methylene blue (MB) with a degradation efficiency of ~93% and ~85% under UV and visible light irradiation, respectively [30]. On the basis of these results, it is concluded that the use of PDMS as a support for semiconducting materials did not achieve a 100% dye degradation efficiency under natural sunlight conditions. Despite the significant performance by these floating photocatalysts, still there is a more space to fabricate new and advanced photocatalysts in terms of low cost, simple fabrication, high recycle life and efficient (100%) degradation efficiency under the irradiation of natural sunlight. The advantages of using the floating substrate is the lightweight, which enables them to float [31]. Also, an excellent recovery and reusability is achievable by the floating photocatalysts due to improved binding of photocatalyst with the floating material which is mainly controlled by the fabrication process [32]. In addition to that the floating photocatalysts have high possibility to expose themselves to the irradiated light, large surface area for making a contact with dye molecules, high interaction with oxygen gas, and consequently an enhanced photocatalytic performance is achievable [32, 33]. Moreover, silica has been used as a supporting material for dye degradation under illumination of visible light with limited performances [34, 35, 36]. Of particular interest to the current study, we found that the reported floating photocatalysts do not have disinfectant activity to kill the pathogens during the degradation of dyes in wastewater, thus the treated water will require an additional chemical or disinfectant agent to kill the pathogens.

In the contrast to synthetic floating photocatalysts, Dead Sea sponges (DSS) can be considered as a natural source of floating photocatalysts, which exhibits infinite number of benefits such as high antibacterial activity and porosity. Importantly, DSSs have the capability to adsorb the dye due to large micro porosity and can also kill the bacteria during the treatment of wastewater [37]. Moreover, silica is naturally present in the DSS which can support the ZnO functionality towards desired photocatalytic processes. To the best of our knowledge, these advantageous aspects of DSS have not been investigated for the degradation of organic dyes. Therefore, DSS can be considered as a renewable natural resource and eco-friendly floating substrate for binding of ZnO particles for quantitative (100%) photo-degradation of MB and simultaneously act as a disinfectant for

pathogens. Additionally, based on the natural disinfecting properties, Dead Sea sponge is considered as renewable photocatalyst with ZnO in this study.

In this contribution, we have employed DSS for the immobilization of ZnO nanosheets using hydrothermal approach and the fabricated ZnO/DSS hybrid material is characterized by scanning electron microscopy (SEM), X-ray diffraction (XRD), energy dispersive spectroscopy (EDS), Fourier transform infrared (FTIR) and UV-Visible spectroscopy techniques and used as a floating photocatalysts, which gave rise almost 100% degradation of MB under illumination of sunlight and excellent recycle life and reusability.

2. Experimental Work

2.1.Materials

The sponge was used as floating substrate for the immobilization of ZnO and the disinfection agent and purchased from supplier Marquee Dead Sea Spa (USA). Zinc acetate dihydrate ($ZnC_4H_6O_4$, M=183.48, Merck), ammonia hydroxide (25%, Merck), ethylenediamine tetracetate (EDTA), ascorbic acid, sodium borohydride, and methylene blue were of analytical grade. All the required solutions were used in the synthesis of the composites in deionized water without further purification.

2.2. Synthesis of ZnO immobilized nanostructures onto Dead Sea Sponge

Initially, the biomass of sponge was washed with double distilled water in order to remove the fine gravels and salt then put into the electric oven at 50 ^oC for dehydration for overnight. Finally the biomass was ready for further experimental process. Zinc acetate dihydrate precursor (2.224g), different weight of the sponge (1g, 2g and 4g) and 5mL ammonium solution were dispersed in 100 mL of DI water. Then, the mixture was transferred into separate (250 mL by volume) beakers and were named as sample-1, sample-2 and sample-3. Whereas, one beaker was containing the precursors without sponge. After that, the beakers were covered with the aluminum foil and subjected to preheated electric oven at 95 ^oC to for 5 hours to get ZnO coated sponge. Finally, the ZnO coated sponge was achieved by filtration and washing with DI water and dried at room temperature for specific period of time for further characterization. The crystal arrays of prepared nanostructured materials was investigated with Philips's powder diffractogram technique under the measurement conditions of CuKα radiation (λ = 1.5418 Å), 45 kV and 45 mA. The morphology

was studied at 3 kV and' to ' Scanning electron microscopy with a ZEISS Gemini SEM 500 equipped with field emission gun. Fourier transform Infra read spectroscopy was used to evaluated the chemical features of ZnO, and the methylene degradation verification using Bruker IR spectrophotometer with sweeping frequency of 400-4000 cm^{-1}. The Uv-visible spectrophotometer was employed to record the absorption spectra at room temperature.

2.3. Photocataytic properties of ZnO immobilized Dead Sea Sponge (DSS).

The photcatalytic behavior of ZnO coated sponge was done on the degradation proportions of methylene blue dye under the natural sunlight source. At first, synthesized ZnO coated sponge (5mg, 10mg and 15mg) were transferred into 50mL of 2.50 $\times 10^{-5}$ M of methylene dye solution. The degradation experiment was accomplished by magnetic starring in the dark for 30 min after achieving adsorption/desorption equilibrium state of methylene blue (MB) dye on the catalytic surface. Then, degradation test of MB dye was conducted with natural sun light at different time interval (20-160 min). The UV-Vis spectrophotometer (lambda 365) was used to measure the residual concentration of MB after each test and the dye removal percentage (%) was calculated as below

$$\text{Dye removal \%} = \frac{Co - Ct}{Co} \times 100 \qquad (1)$$

Where Co and Ct are the MB absorbance before degradation and final absorbance of dye at different time intervals "t," of natural light irradiation respectively.

Recyclability of ZnO immobilized onto 4 grams of DSS with catalyst dose of 15 mg was evaluated by several cycles under natural sunlight for the degradation of methylene blue (MB) dye. The reusability tests were conducted five times considering the irradiation time of 270 min, the MB concentration of 2.50 $\times 10^{-5}$ M, volume of dye 50 mL, the catalytic dose of 15mg. After each test, the ZnO coated sponge was comprehensively washed with DI water, dried at room temperature for specific period and used over again for the subsequent run.

The trapping experiment was accomplished by using three reagents to detect the reactive species in the photocatalytic degradation. Different scavengers such as ascorbic acid ($C_6H_8O_6$ $\cdot O^{2-}$ scavenger), ethylenediamine tetraacetate acid disodium (EDTA-Na_2 h^+ scavenger) and sodium monohydrate ($NaBH_4$, $^{\cdot}OH$ scavenger) were employed. The trapping agents were introduced to MB solution and the concentration of each was 0.1 mol l^{-1}.This experiment was conducted for 180

min under the natural sun light in the presence of 15mg of the ZnO immobilized onto 4 grams of DSS.

2.4. Antibacterial activity study of pure sponge, pure ZnO and ZnO immobilized on 4 gram of DSS

The potential of hydrothermal synthesis ecofriendly ZnO coated sea dead sponge nanomaterial to kill bacterial pathogen such as *E. coli* and *P. areuginosa* was tested using the well diffusion method. The culture of said bacteria were swabbed uniformly on the nutrient agar media for 24 h at 37^{o}C. After 24h of incubation, the bacterial analysis was performed by using inoculum of overnight culture of each bacterial species grown on Mueller Hinton Broth (MHB). After that the inoculum was carefully distributed on a Mueller Hinton Agar petri dish in a constant manner. The wells were made using a sterile cork borer (6mm in diameter) into agar plates possessing inoculums (bacterial suspension). The known concentration of 60 µl of pure ZnO and ZnO coated sponge were placed into the wells respectively. The plates were placed at 36 ^{0}C for 24h for successive incubation. After incubation, the zone of inhibition of bacteria was observed in mm scale which was formed around the well. A10 mg powder of pure DSS, pristine ZnO and ZnO/DSS hybrid photocatalyst was used to make a slurry in the deionized water using ultrasonic bath for the uniform photocatalyst solution. Then, 10µL with a mass of (0.2mg) of photocatalyst slurry was dropped onto glassy carbon electrode using drop casting methodology. The cleaning of glassy carbon electrode was done with alumina paste and silicon paper followed by washing with the deionized water. After cleaning and washing, it was dried at room temperature. The modified glassy carbon electrode was used to record impedance spectra of pure DSS, pristine ZnO and ZnO/DSS hybrid photocatalyst against silver-silver chloride (Ag/AgCl) and counter electrode of platinum wire using a sweeping frequency range 100 kHz to 1 Hz at zero bias potential and amplitude of 10 mV. The impedance spectra of each material were recorded in the MB 2.50 $\times 10^{-5}$ M solution at room temperature. The experimental results of impedance were fitted with Zview software.

3. Results and discussion

3.1. Aspects of morphology, composition and crystallinity of ZnO immobilized onto Dead Sea sponge (DSS)

The detailed information about the synthesis, structural characterization and the functionality of prepared materials is enclosed in Supplementary Information. A schematic diagram is illustrating the deposition of ZnO onto the DSS by hydrothermal process as shown in Supplementary Information (S1). The digital images of degradation performance of pure MB concentration of 2.50×10^{-5} M without catalyst, 15 mg catalyst dose of bare DSS, pure ZnO and ZnO immobilized onto 1, 2 and 4 grams of DSS in MB concentration of 2.50×10^{-5} M with the illumination of natural sunlight at time interval of 160 min are enclosed in Figure 1. This is confirming the physical evidence of the presented study towards the 100 % degradation of MB. The ZnO immobilized onto DSS could be regarded as new functional floating photocatalyst for the complete degradation of MB from aqueous solution and considered a solution towards the wastewater treatment.

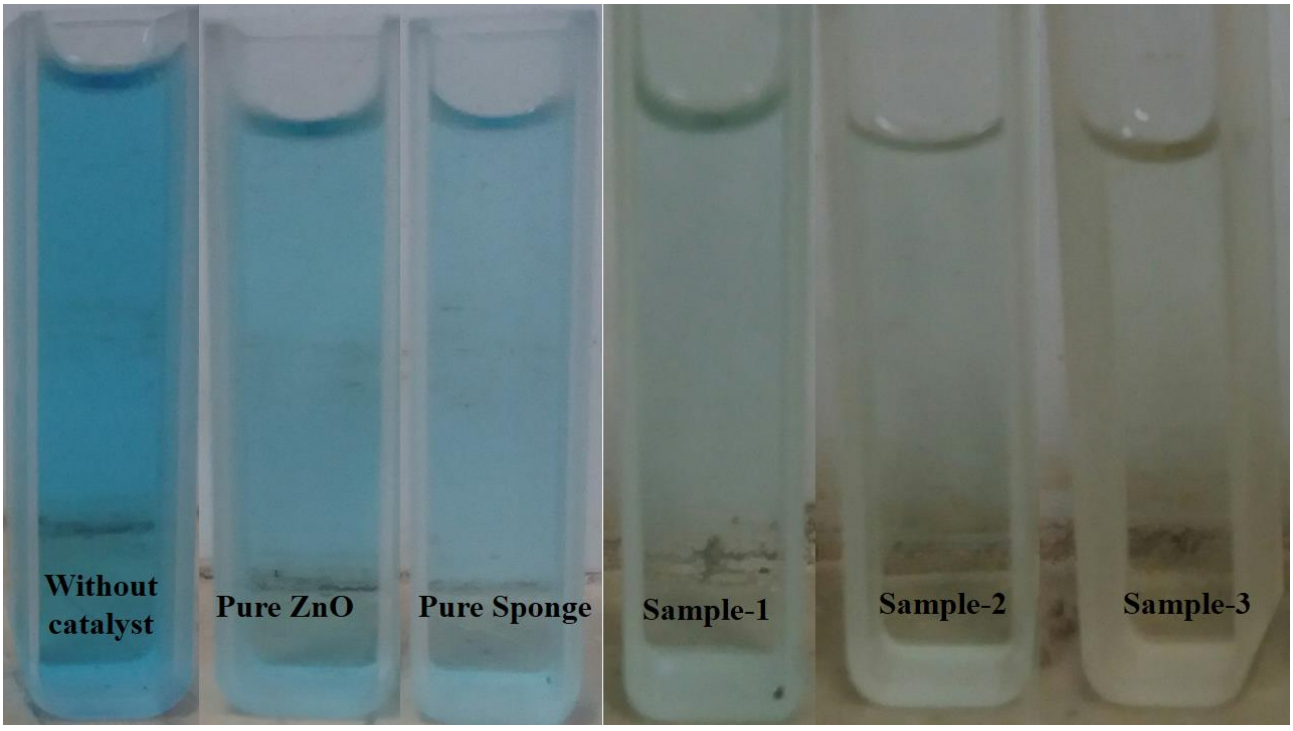

Figure 1: Digital images of degradation process, from left dye solution of 2.50×10^{-5} M without catalyst, and 15 mg catalyst dose of pure ZnO, pure DSS and ZnO immobilized onto 1, 2 and 4 grams of DSS in MB concentration of 2.50×10^{-5} M for the time interval of 160 min under the illumination of sunlight.

The morphology of pure ZnO, bare DSS and ZnO/DSS (4 grams of DSS) were probed by low resolution SEM as depicted in Figure 2. The bare DSS exhibits micro skeleton-like structure containing large pores as shown in Figure 2a. The pure ZnO is characterized by randomly oriented nanorod-like morphology with approximate length of 6-7 microns with average diameter ~ 2-3 microns as shown in Figure 2b. After the immobilization of ZnO onto DSS, the morphology of ZnO is evolved from nanorod to nanosheets as evident under different magnifications (Figure 2c-e). It is obvious from Figure 2c that DSS is fully covered with ZnO nanostructures and the morphology of ZnO seems as a flower like as shown in Figure 2d. Further increasing the magnification, it is seen that flowers are composed of thin nanosheets with wall thickness as shown in Figure 2e. The low resolution SEM images of ZnO/DSS hybrids onto 1 and 2 grams of DSS are shown in Supplementary Information (S2a-b), indicating the significant amount of immobilization of ZnO onto them. Also, the SEM images of ZnO/DSS hybrid material is enclosed in (S2c-d), revealing almost similar morphology and well attachment of ZnO onto DSS.

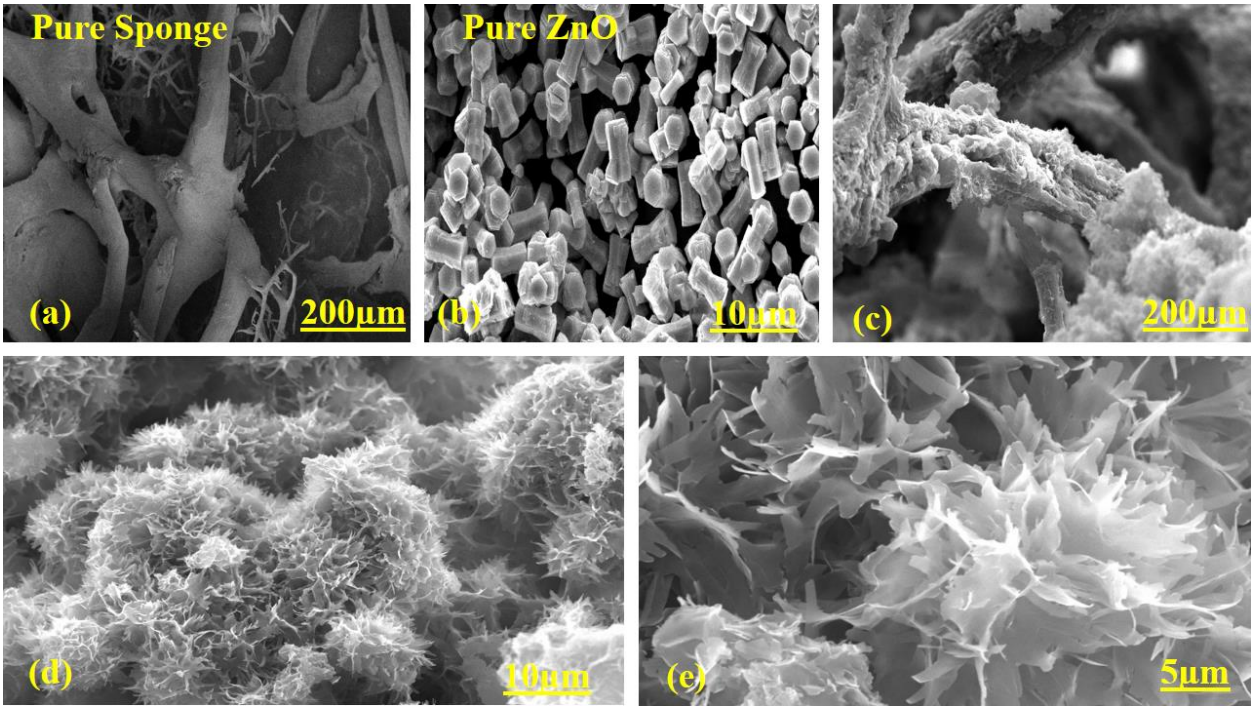

Figure 2: SEM images (a) bare DSS, (b) pure ZnO, (c,d,f) ZnO immobilized onto 4 grams of DSS

The elemental composition of various samples of ZnO immobilized onto 1, 2, and 4 grams of DSS as a support were investigated by EDS analysis as shown in Supplementary Information (S3). The major elements were Zn, O Si, Ca, Mg and C as depicted in Supplementary (S3a-c). The EDS analysis revealed that the composition of floating photocatalyst is mainly consisting Zn and O in addition to the several chemical elements commonly found in the Sea Sponge due to presence of high density of variety of salts in the sea water. The EDS elemental mapping was also performed on the ZnO/DSS hybrid material prepared with highest amount of DSS as shown in Supplementary (S4). It is clear that the identified elements are uniformly distributed and relative distribution of Zn and O is higher than elements indicating the homogenous immobilization of ZnO nanosheets onto DSS.

Figure 3a displays the XRD patterns of pure ZnO and various ZnO immobilized onto 1, 2 and 4 grams of DSS samples. The measured diffraction patterns of pure ZnO sample are highly intense and located at 31.77^{o}, 34.42 ^{o}, 36.25 ^{o}, 47.53 ^{o}, 56.60 ^{o}, 62.86 ^{o}, 66.38 ^{o}, 67.96 ^{o}, 69.10 ^{o}, 72.56 ^{o} and 76.95 ^{o}, and corresponded to (100), (002), (101), (102), (110), (103), (200), (112), (201), (004) and (202) crystal planes respectively. The XRD reflections of pure ZnO are correlated

to hexagonal wurtzite structure and well supported by (reference code: 00-036-1451). However, in case of ZnO immobilized onto DSS samples, the various diffraction patterns of SiO_2 in addition to ZnO are confirmed at 26.59 °, 38.38 °, 50.51 °, 59.85 °, 65.67 °, 73.29 ° and 75.51° assigned to (101), (012), (003), (211), (300), (014), (032) and (022) crystal planes respectively. This indicates that the composition of ZnO immobilized onto DSS is mainly based on the ZnO and SiO_2. The intensity of ZnO reflections is slightly decreased and it could be indexed to evolution of morphology from nanorod to nanosheets and the nanosheets are heterogeneously decorated on the DSS. Figure 3b shows the fitting analysis done to the plane of (100), (002) and (101) at 2θ (°) and it is obvious that the diffraction patterns are inclined toward higher angle and consequently a slight variation in the lattice parameters can visualized from Figure 3b. The shifting of two theta angle towards higher value is attributed to inter-planar distance of various (100), (002) and (101) crystal planes at 2θ (°), suggesting excellent crystalline characteristics. Interestingly, the shift of two theta has significant influence on the lattice parameters and volume of unit cell of ZnO nanostructures.

Generally, tensile and compression microstrains have been noticed for the shift in XRD patterns to higher and lower two theta angle [38]. Furthermore, the peak shift towards higher angle provides the scenario of particles of nm range, size of the diffraction reflection would be highly diffusive and broadened. Also, the reflection of crystal structure at their surface structure would be highly randomly oriented[38].

The chemical bonding of pure MB Zn-O, and Sponge was investigated by FTIR technique as shown Figure 4 (a, b). In ZnO, the typical metal-oxygen stretching vibration modes are ascribed between 430-600 cm^{-1} [39] as shown in Figure 4a. The intense absorption peaks at 1434, 1448, 3422, 3444 and 3451 cm^{-1} are particular absorption bands of hydroxyl groups of adsorbed water molecules on the surface of samples [40] as shown in Figure 4a. Furthermore, the vibrations from 2850-2930 cm^{-1} are assigned to adsorbed CH_3COO^- ions adsorbed don the surface of ZnO during the synthesis of ZnO from zinc acetate di-hydrate precursor. In case of pure MB, two functional groups like –NH/-OH were interfered at 3347 cm^{-1}, the peak at 2714 cm^{-1} is labeled for stretching vibration of –CH- aromatic and $–CH_3$ methyl groups. The bands of ranging from 1590-1332 cm^{-1} are attributed from aromatic ring structure in MB [41,42]. The band at 1250 cm^{-1} is assigned to the C=C skeleton of aromatic rings of MB. Other C–S–C at 1037 cm^{-1} and the out of plane are connected ranging from 880 -805 cm^{-1} bending vibrations as shown in Figure 4b. These most of

the FRIR bands are typical features ascribed to chemical bonding of pure MB. In bare sponge, intense absorption at 1163 cm^{-1} was indexed to longitudinal optical band of Si-O-Si indicating the asymmetric stretching frequencies [43] as shown in Figure 4c. A highly intense and broad signal measured at 1086 cm^{-1} is attributed to transversal optical absorption band of Si-O-Si coming asymmetric stretching frequency [44]. Beside this, symmetric stretching modes of Si-O-Si appeared at 878 cm^{-1}, followed by its bending vibration at 469 cm^{-1}. A peak appeared at 716 cm^{-1} is corresponded to Si-O stretching mode of SiO_2 [45] as shown in Figure 4c. The bare DDS sponge is mixture of spongin and spicules. The spicules are mainly composed of calcium carbonate and silica. However, the spongin are modified version of collagen protein. Therefore, the vibrating bands ranging from 2850-2930 cm^{-1} in bare DSS are possibly assigned to collagen protein, but it needs more detailed FTIR studies on chemical bonding of DSS. After the immobilization of ZnO onto DSS, the FTIR study has shown the characteristic peaks for both ZnO and SiO_2 as shown in Figure 4d. Before the dye degradation, the typical peaks of Si-O-Si are observed at 882 cm^{-1} due to asymmetric frequency and the absorption peak at 1026 cm^{-1} is corresponded to Zn-O-Si vibrational modes [46]. The typical stretching modes for the immobilized Zn-O are appeared at 471-529 cm^{-1} as shown in Figure 4d. The vibrating bands for the region 2850-2930 cm^{-1} are slightly shifted due to interaction of ZnO with DSS and they could be possibly assigned to zinc acetate precursor and collagen protein part of DSS. After the degradation of MB on the surface of ZnO immobilized onto DSS, many of the bands are disappeared confirming the successful degradation reaction on the presented composite material as shown in Figure 4d.

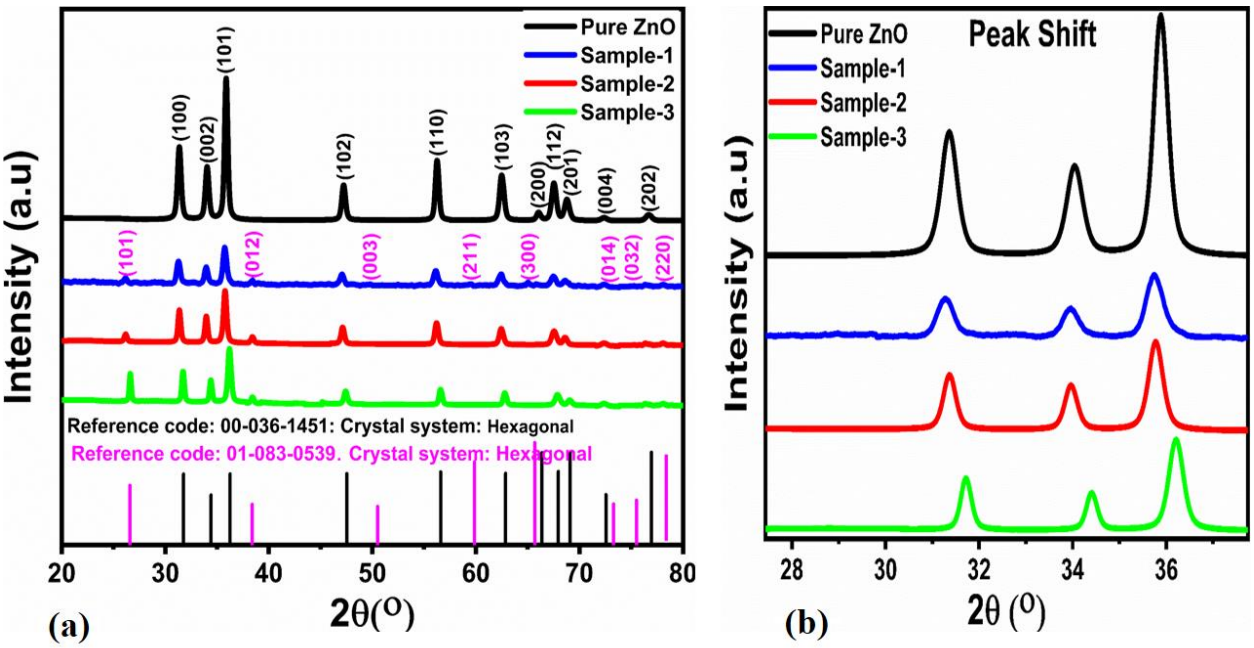

Figure 3: XRD Patterns (a) bare DSS, pure ZnO, ZnO immobilized onto 1, 2 and 4 grams of DSS, (b) Peak shift analysis

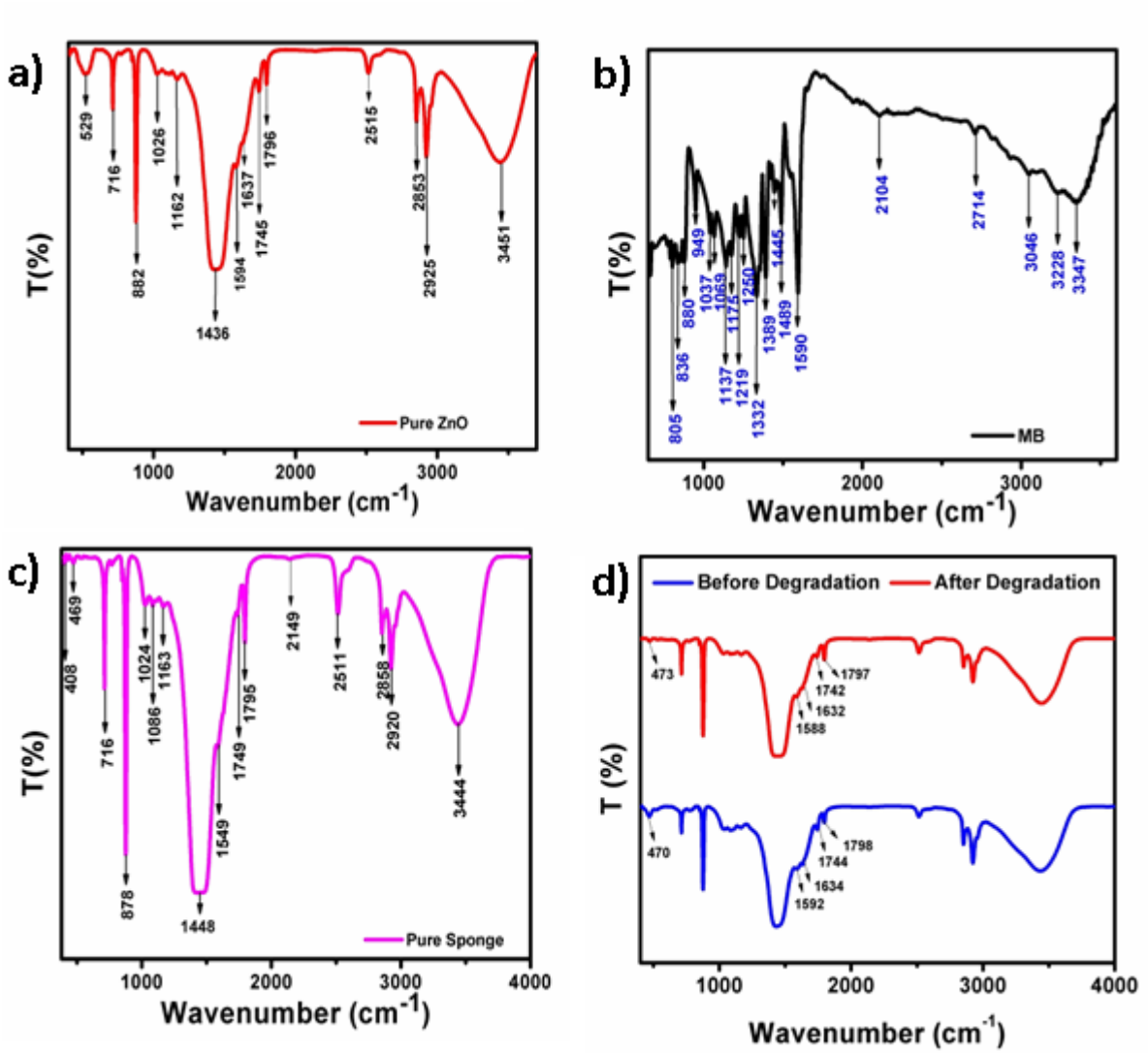

Figure 4: (a) FTIR absorption spectra of pure ZnO and MB, (b) FTIR spectra of pure DSS, (c) FTIR absorption spectra of ZnO immobilized onto DSS before and after the degradation of MB

3.2. Photodegradation of MB by various ZnO immobilized onto 1, 2 and 4 grams of DSS samples under Sunlight illumination

Various samples of ZnO immobilized onto 1, 2 and 4 grams of DSS for the photodegradation of MB considered as a model dye in aqueous solution under the illumination of natural sunlight were used. The visual images of ZnO immobilized onto 1, 2, and 4 grams of DSS as a floating photocatalyst are enclosed in Supplementary Information (S5) indicating the effectiveness of DSS as a floating substrate. Also, the deposition amount of ZnO particles onto the 1, 2 and 4 grams of

DSS was found in in increasing order for the catalyst dose of 5, 10 and 15 mg of each sample as shown in Supplementary Information (S6). To understand the photocatalytic activity of prepared materials, the degradation was examined under the dark conditions using catalyst dose of 15 mg of pure ZnO, bare DSS and 15 mg of ZnO/DSS hybrid on 4 grams of DSS and dye concentration of 2.50 $\times 10^{-5}$ M as shown in Supplementary Information (S7a-d). This study indicates a poor catalytic activity, suggesting the adsorption of MB onto the materials instead of oxidation reaction. Also, the degradation kinetics is poorly shown with very a limited degradation efficiency as enclosed in Supplementary Information (S8a-b).

The UV-visible absorbance spectra of MB solution without the photocatalyst, with 15 mg catalyst dose of pure ZnO and bare DSS in dye concentration of 2.50 $\times 10^{-5}$ M at different time intervals and under irradiation of natural sunlight are enclosed in Supplementary Information (S9a-c). It can be seen from the absorbance values that the decrease in dye concentration is very slow and the corresponding degradation efficiencies for the MB without photocatalyst, pure ZnO and bare DSS were found as 42.10, 56.16, and 62.68% respectively for the period of 5 hours as shown in Supplementary (S9d). These performances confirmed that the pristine materials are more active under the illumination of natural sunlight than the dark conditions. The degradation kinetics was also studied for the pure ZnO, bare DSS and the dye solution without the photocatalyst as enclosed in Supplementary Information (S10a-b). The kinetics analysis again confirms that the DSS has superior capability to accelerate the degradation rate with a rate constant value of 2.14×10^{-3} min^{-1}, whereas pure ZnO has shown degradation rate constant of 1.61×10^{-3} min^{-1} and the dye solution without catalyst has a shown rate constant of 7.32×10^{-4} min^{-1} and followed by the pseudo first order kinetics. This indicates that the degradation efficiency of bare DSS for MB was observed higher than pure ZnO and pure MB solution due to combined effect of adsorption of porous structure and the oxidation of MB by the presence of SiO_2 within the composition of bare DSS [47]. The low degradation efficiency of pure ZnO for MB is according to the reported work [48], and the several reasons impair the degradation efficiency of pure ZnO such as morphology, the adapted synthetic process for pure ZnO, and the wide band gap which allows the fast charge recombination rate of electron and hole pairs within the pure ZnO during the illumination of light. ZnO with PDMS sponge with a catalysts dose of 600 mg has shown 85% degradation efficiency for MB has been reported[48] and still it tells us that the new functional materials have to be designed for the 100% removal of dyes from the wastewater [48]. The immobilization of ZnO on various amounts of

DSS such as 1, 2 and 4 grams was carried out for the illustration of role of Sponge towards the enhancement of photocatalytic activity of ZnO. The degradation performance in terms of UV-visible absorbance spectra of 5 mg of catalyst dose of ZnO immobilized onto 1, 2 and 4 grams of DSS towards the degradation of MB concentration of 2.50×10^{-5} M under the illumination of natural sunlight and their corresponding degradation efficiency is shown in Figure 5a-d. In first 20 min, about 70% of removal of dye could be contributed to simultaneous adoption and oxidation processes as shown in Figure 5d.

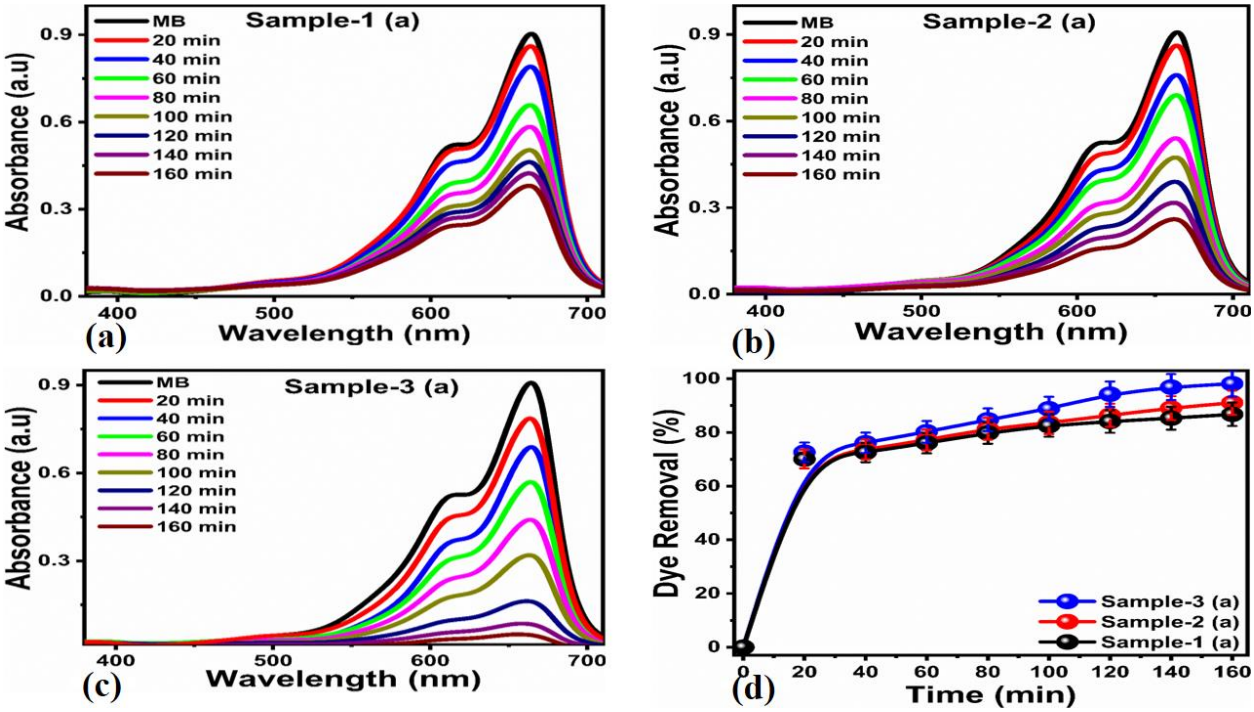

Figure 5: UV-visible absorbance spectra in MB concentration of 2.50×10^{-5} M for the time interval of 160 minutes under the illumination of natural sunlight (a) 5 mg catalyst dose ZnO immobilized onto 1 gram of DSS, (b) 5 mg catalyst dose ZnO immobilized onto 2 gram of DSS, (c) 5 mg catalyst dose ZnO immobilized onto 4 gram of DSS, (d) Degradation efficiency of 5 mg catalyst dose ZnO immobilized onto 1, 2 and 4 grams of DSS.

The 5 mg of catalyst dose of ZnO immobilized onto 1, 2, and 4 grams of DSS contains a loading amount of ZnO as 5.35×10^{-4}, 8.075×10^{-4}, and 8.425×10^{-4} grams respectively, suggesting that large size of DSS could deposit high amount of ZnO. It can be seen that the degradation activity of MB was enhanced by the immobilization of ZnO onto various amounts of DSS by using 5 mg of

catalyst dose. It confirms that the use of higher amount of floating substrate of DSS has revealed an increasing trend towards the Photodegradation of MB under natural sunlight as shown in Figure 5a-c. The measured degradation efficiency of 86.74, 91.06, and 98.17% towards MB were highly improved by using catalyst dose of 5 mg of ZnO immobilized onto 1, 2 and 4 grams of DSS respectively as enclosed in Figure 5d. A large amount of ZnO was immobilized onto 4 grams of Sponge which increased the degradation performance compared to the ZnO immobilized onto 1and 2 grams of DSS. This increase in the performance of prepared hybrid material is assigned to the development of ZnO-SiO_2 nanocomposite on to the surface of porous DSS which decreased the recombination rate and possibly enhanced the electron-hole pair life time through the addition of conduction band electrons from ZnO-to-SiO_2. Interestingly, the presence of SiO_2 within the DSS could effectively separate the photogenerated charge carriers and could uplift the additional active catalytic sites through the interaction of ZnO and SiO_2 itself [49], therefore, outperform functionality towards the degradation of MB is achieved on the ZnO immobilized onto the DSS. Similarly the catalyst dose of 10 mg of ZnO immobilized onto 1, 2 and 4 grams of DSS were studied in dye concentration of 2.50×10^{-5} M and the related degradation efficiencies are enclosed in Figure 6a-d.

The obtained performance of ZnO immobilized on DSS is suggesting that the natural Sea Sponge is an ideal material for the enhancement of the photocatalytic activity of photocatalytic materials like ZnO and it could be considered as a commercial composite material for the practical wastewater treatment problems.

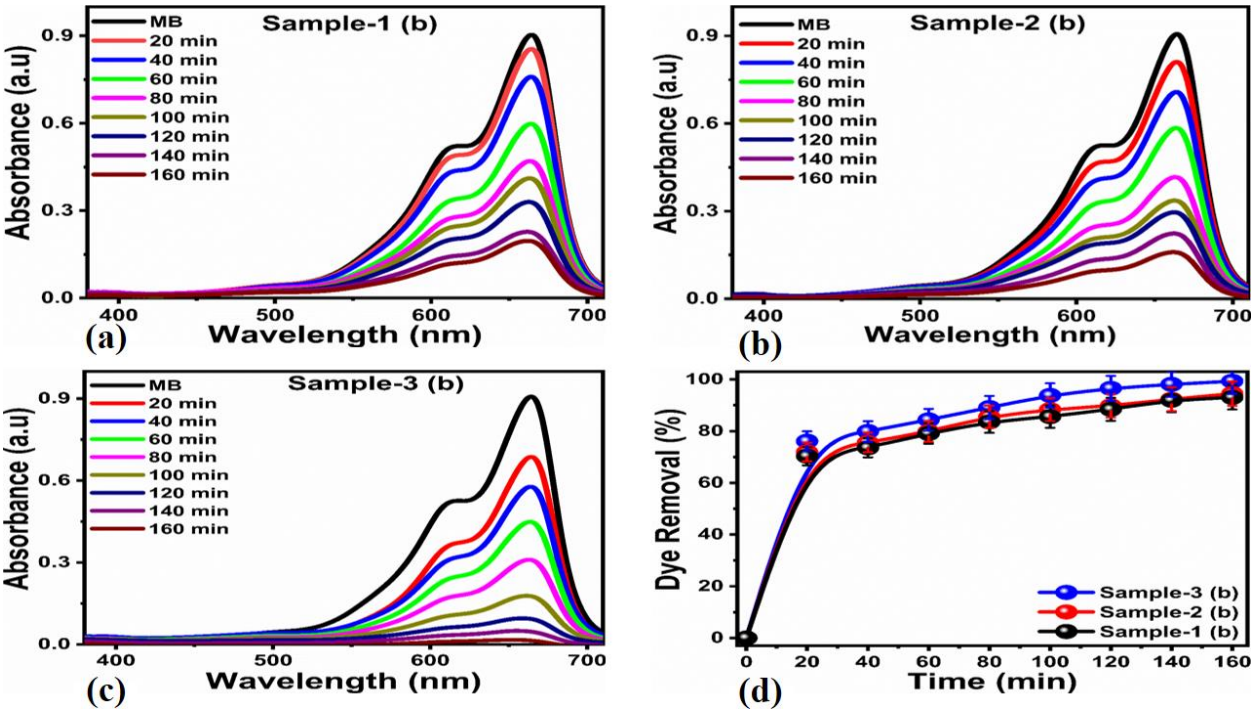

Figure 6: UV-visible absorbance spectra in MB concentration of 2.50 ×10^{-5} M for the time interval of 160 minutes under the illumination of natural sunlight (a) 10 mg catalyst dose ZnO immobilized onto 1 gram of DSS, (b) 10 mg catalyst dose ZnO immobilized onto 2 gram of DSS, (c) 10 mg catalyst dose ZnO immobilized onto 4 gram of DSS, (d) Degradation efficiency of 10 mg catalyst dose ZnO immobilized onto 1, 2 and 4 grams of DSS.

The increased dose from 5 mg to 10 mg has further enhanced the degradation rate and efficiency of using ZnO immobilized onto 1, 2 and 4 grams of DSS. The 10 mg of catalyst dose using ZnO immobilized onto 1, 2, and 4 grams of DSS is loaded with 0.00107, 0.00161, and 0.00169 grams respectively and indicating that increasing the catalyst dose of ZnO immobilized onto 4 grams carried higher amount of ZnO. The degradation efficiency of MB using 10 mg of ZnO immobilized photocatalyst immobilized onto 1, 2 and 4 grams of DSS are obtained as 93.05, 94.51 and 99.32% respectively as shown in Figure 6d. We have further investigated the optimized catalyst dose of 15 mg of ZnO immobilized onto the 1, 2 and 4 grams of DSS in dye concentration of 2.50 ×10^{-5} M and the measured degradation efficiencies are in Figure 10. A catalyst dose 15 mg ZnO immobilized onto 1, 2, and 4 grams of DSS contains 0.00161, 0.00242, and 0.00253 grams respectively. The use of 15 mg of ZnO immobilized onto 4 grams of DSS has confirmed the complete removal of MB from aqueous solution as shown in Figure 7a-c. The observed

degradation efficiencies of 15 mg of ZnO immobilized onto 1, 2 and 4 grams of DSS are 95.16, 95.95 and 99.94% are shown in Figure 7d. This study is revealing that the lowest amount of 0.00253 grams for ZnO was deposited on the 15 mg catalyst dose of ZnO immobilized onto 4 grams of DSS to be used to date for 100% degradation efficiency of MB from aqueous solution under the illumination of sunlight. The design and architecture of DSSs as floating substrate is illustrating that unique features for the development of new generation and functional photocatalysts for the chronic environmental issues. From this analysis, it is obvious that ore for the first time we report the immobilization of ZnO nanosheets onto DSS and the prepared hybrid material with a dose of 15 mg has performed dramatically towards 100% degradation of MB in dye concentration of 2.50×10^{-5} M. The degradation efficiency enclosed in Figure 5d, 6d and 7d is triplicated and average with error bar is shown in S11, suggesting a slight increase in the efficiency with increasing catalyst dose of same sample like sample 1, sample 2 and sample 3.

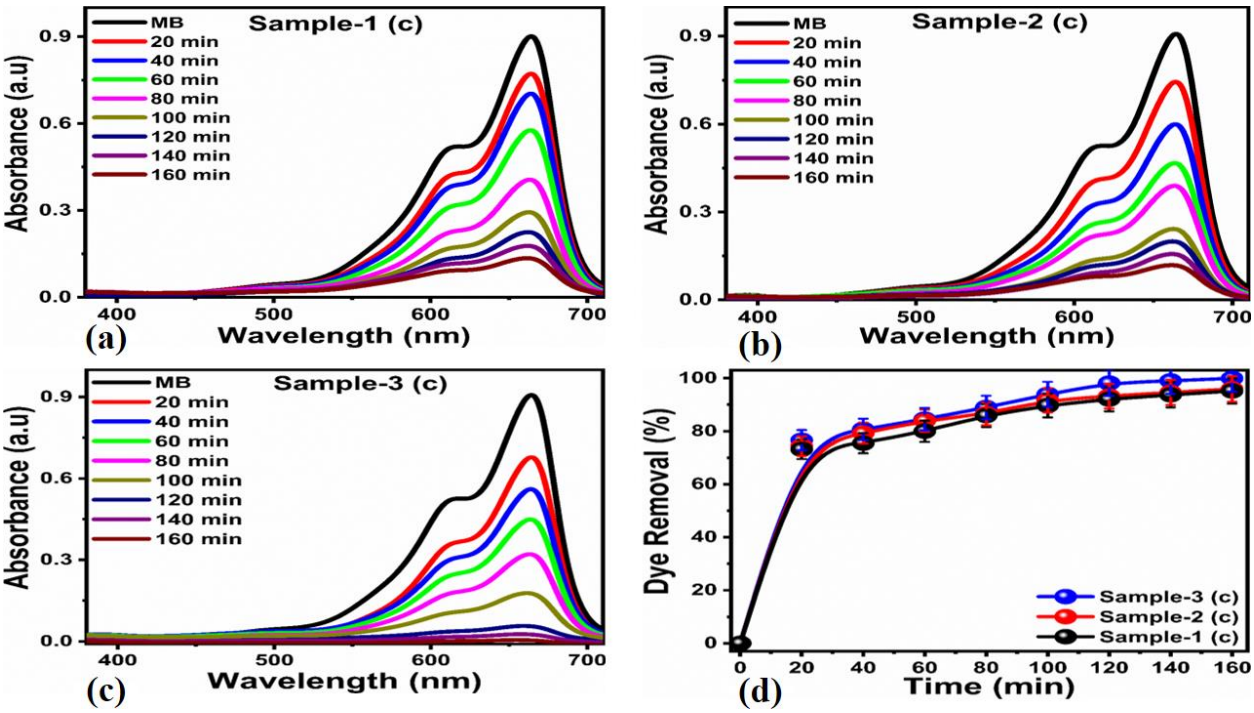

Figure 7: UV-visible absorbance spectra in MB concentration of 2.50×10^{-5} M for the time interval of 160 min under the illumination of natural sunlight (a) 15 mg catalyst dose ZnO immobilized

onto 1 gram of DSS, (b) 15 mg catalyst dose ZnO immobilized onto 2 gram of DSS, (c) 15 mg catalyst dose ZnO immobilized onto 4 gram of DSS, (d) Degradation efficiency of1 5 mg catalyst dose ZnO immobilized onto 1, 2 and 4 grams of DSS,

The kinetics was also evaluated for the 5 mg catalyst dose of ZnO immobilized onto the 1, 2 and 4 grams DSS toward degradation rate of MB as shown in Figure 8a. The degradation rate constant values were estimated as 5.81×10^{-3} min^{-1}, 8.09×10^{-3} min^{-1}, and 1.779×10^{-2} min^{-1} for the catalyst dose of 5 mg ZnO immobilized onto the 1, 2 and 4 grams of DSS as a substrate. The kinetics of 5 mg of catalyst dose was highly increased for the degradation reaction of MB and indicating as superfast simultaneous adsorption and oxidation process of MB on the surface of ZnO immobilized ZnO 4 grams of DSS. The degradation kinetics of 10 mg dose of catalyst of ZnO immobilized onto the 1, 2, and 4 grams of DSS was also monitored as enclosed in the Figure 8b. The calculated rate constant values are 9.98×10^{-3} min^{-1}, 1.098×10^{-2} min^{-1}, and 2.288×10^{-2} min^{-1} for the 10 mg of ZnO immobilized onto 1, 2 and 4 grams of DSS respectively. A catalyst dose of 10 mg of ZnO immobilized onto 4 grams of DSS has revealed an outstanding degradation kinetics. The measured kinetic study is further revealing that the catalyst dose is essential to optimized and it has a great impact on the degradation kinetics of MB as proven in this study and other reported works. The kinetics of 15 mg catalyst dose of ZnO immobilized onto 1, 2 and 4 grams of DSS was also studied as shown in Figure 8c and the measured rate constants values for the degradation of MB are 1.231×10^{-2} min^{-1}, 1.316×10^{-2} min^{-1} and 3.351×10^{-2} min^{-1} respectively. The high rate constant value of 3.351×10^{-2} min^{-1} and the degradation efficiency of 99.94% for the 15 mg of catalyst dose of ZnO immobilized onto 4 grams of DSS in MB concentration of 2.50×10^{-5} M for the time interval of 160 min are the advantageous features of the proposed study. For better understanding the rate constant values for the degradation reaction on the surface of ZnO immobilized onto 1, 2 and 4 grams of DSS with a catalyst dose of 5, 10 and 15 mg of each sample in MB concentration of 2.50×10^{-5} M are enclosed in Supplementary Information (S12). The reaction kinetics for the degradation of MB on the surface of ZnO immobilized onto DSS is followed by pseudo first order kinetics as witnessed by the fair rate constant values. The amount of DSS as a floating substrate, the catalyst dose and initial dye concentration are the critical parameters evaluated for the fabrication of ZnO based photocatalyst for 100% degradation efficiency towards MB. The degradation reaction profile at MB concentration of 2.50×10^{-5} M under the illumination of sunlight is enclosed in Figure 8d-f. The use of 5 mg of ZnO immobilized onto 1, 2 and 4 grams of DSS

have shown improved photocatalytic activity of MB which could be assigned to firm binding of ZnO nanosheets onto the Sponge substrate. The catalyst dose of 5 mg of ZnO immobilized onto 4 gram DSS has revealed about 98.17% as shown in Figure 8d. Moreover, the reaction rate profile for the 10 mg of ZnO immobilized onto 1, 2 and 4 grams of DSS is enclosed in Figure 6e and suggesting approximately 99.32% degradation efficiency. For the sample of ZnO immobilized onto 1, 2 and 4 grams of DSS with a catalyst dose of 15 mg the reaction profile for the degradation of MB is enclosed in Figure 8f. The measured degradation efficiency of 99.94% is indicating almost complete removal of MB from the aqueous solution. Figure 8f for the sample 3 is further re-plotted and shown in S13 for the recalculation of rate constants of MB degradation. The recalculated rate constants are shown in Table S1. It has shown that there are two regions for the degradation process, confirming the decomposition of MB into secondary constitutes. The data of the S13 seems that there are two different slopes (i) for the time period 0 to 80 mins and (ii) from 100 to 160 mins. The linearity of the data is confirmed from R squared values shown in the inset. This probably suggests that during the degradation MB dye is converted to secondary organic product which starts its degradation from the time 100 mins and completely degraded after 160 mins as shown in S13. The data of all three samples i.e. Sample 3 a-c is shown in S13 which clearly shows that the obtained experimental data could not follow the linearity. In order to have a best understanding, the obtained data is divided into two regions and the mathematical model describing the straight line is best fit to the data. The values of the rate constant are also calculated from each linear part of the data and the average (K) values are mentioned in the Table S1 which elucidate that the maximum K- value is obtained for sample 3(c).

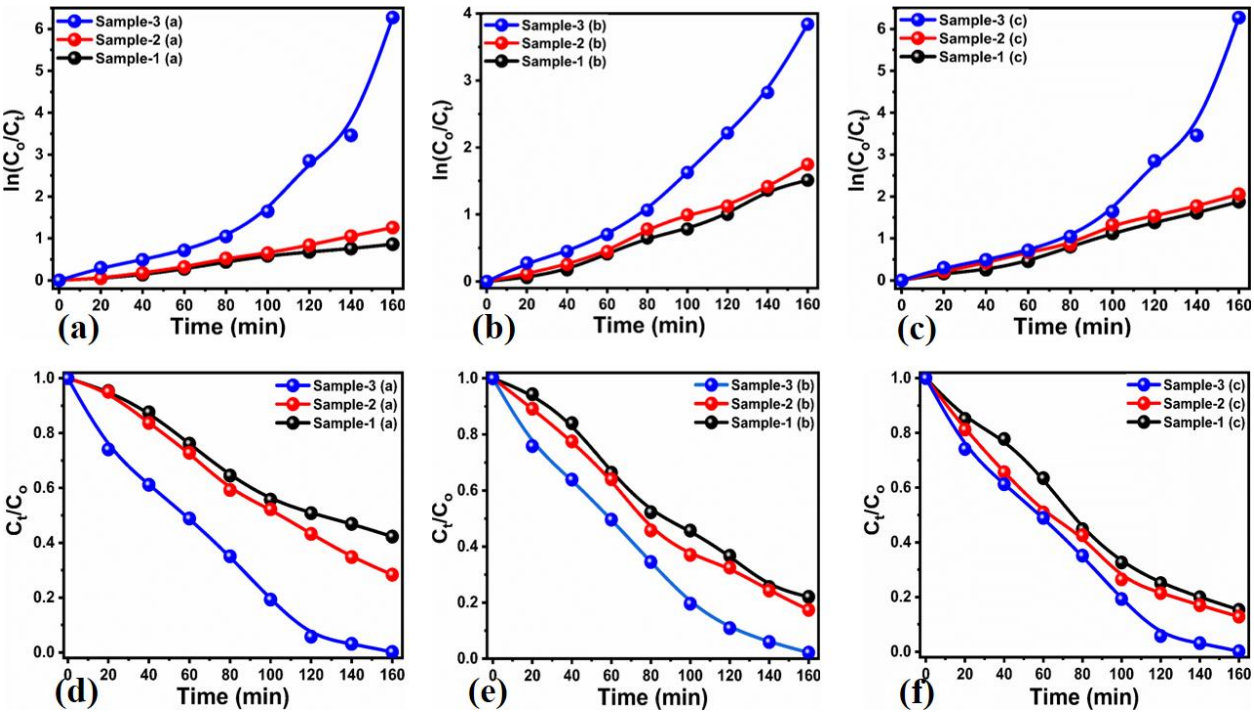

Figure 8: Linear plotting for kinetic versus different time intervals in MB concentration of 2.50 $\times 10^{-5}$ M for the time interval of 160 minutes (a) 5 mg catalyst dose of ZnO immobilized onto 1, 2 and 4 grams of DSS, (b) 10 catalyst dose ZnO immobilized onto, 1, 2 and 4 grams of DSS, (c) 15 mg catalyst dose ZnO immobilized onto 1, 2 and 4 gram of DSS, (d) Photodegradation reaction profile for MB concentration of 2.50 $\times 10^{-5}$ M for the time interval of 160 min for 5 mg catalyst dose of ZnO immobilized onto 1, 2 and 4 grams of DSS, (e) 10 catalyst dose ZnO immobilized onto, 1, 2 and 4 grams of DSS, (f) 15 mg catalyst dose ZnO immobilized onto 1, 2 and 4 gram of DSS

Furthermore, the detection of major reactive substances during the photocatalysis of MB was carried out in order describe the degradation mechanism on the surface of ZnO immobilized onto DSS. As we used the photodegradation of MB on various ZnO immobilized onto DSS under the irradiation of natural sunlight. The photocatalysis is started through the production of electron-hole pairs, then these electron hole pairs are involved in the generation of reactive $O_2^{-\cdot}$ and $^{\cdot}OH$ radicals followed by oxidation of organic dye [50, 51]. It has been shown that the water based generation of hydrogen atoms are responsible for the decline in the degradation process of dye, therefore we studied the scavenger role during the same conditions of photocatalysis of MB. The addition of ethylenediamine tetracetatete (EDTA), ascorbic acid and sodium borohydride (NaBH4) as scavengers could create a stress at the equilibrium of photodegradation of MB using ZnO

immobilized onto DSS. The effect of radical and ion introducing substances was studied as enclosed in Figure 9. In the scavenger study, we aimed to see the suppression effect of particular scavenger agent on the density of superoxide radical ions ($^{\bullet}O^{-}_{2}$), hydroxyl radicals ($^{\bullet}OH$), and photogenerated holes (h^{+}), which are actively involved in the degradation process. The ascorbic acid, sodium borohydride and ethylenediamine tetracetate (EDTA) have direct influence on ($^{\bullet}O^{-}_{2}$), and hydroxyl radicals ($^{\bullet}OH$) [52]. The degradation of MB is mainly governed by these oxidizing agents as reported by previous studies [53, 54], therefore we mainly focused on these scavenger agents in the proposed study. The decrease in the degradation efficiency was very prominent for ascorbic acid compare to the degradation of MB without scavenger.

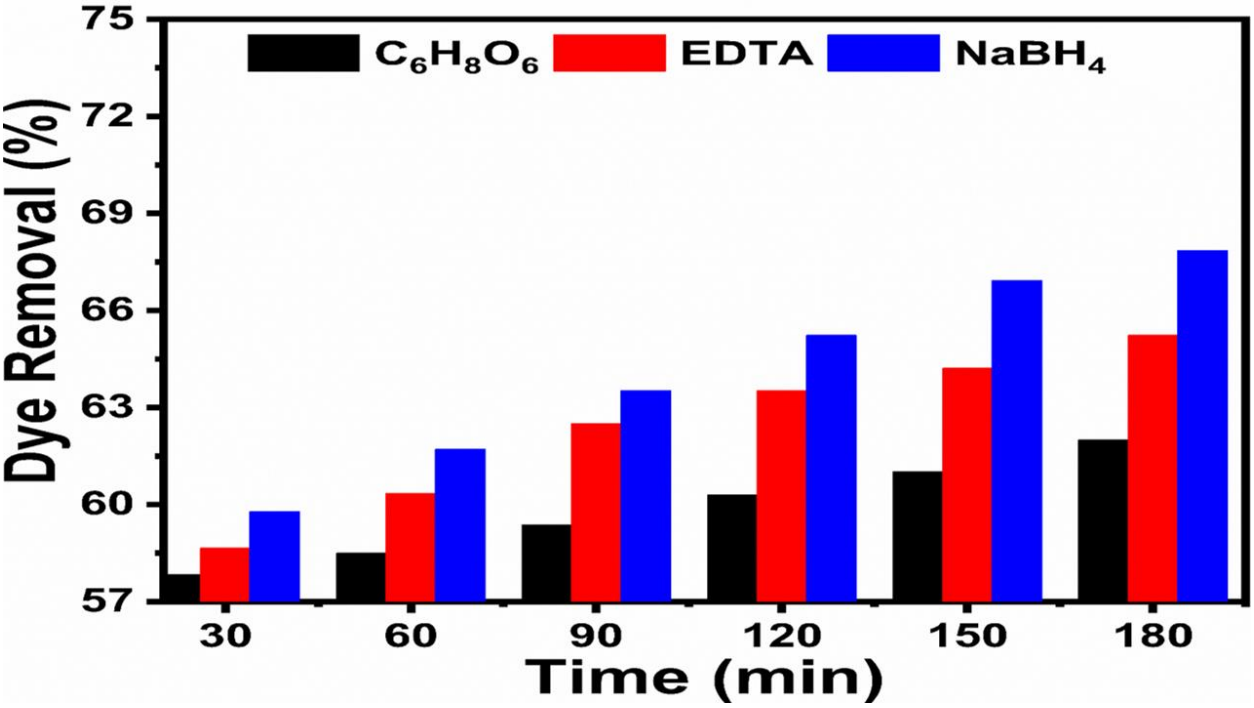

Figure 9: Photodegradation of MB under the influence of various scavengers in MB concentration of 2.50 $\times 10^{-5}$ M using 15 mg catalyst dose of ZnO immobilized onto 4 grams of DSS under the illumination of sunlight.

The activity of various ZnO immobilized onto 1, 2 and 4 grams of DSS was also investigated in higher MB concentration of 3.4×10^{-5} M under the illumination of natural sunlight as shown in Supplementary (S14). It can be seen that by increasing dye concentration from MB concentration

of 2.50 $\times 10^{-5}$ M to 3.4×10^{-5} M, the effectiveness of ZnO immobilized onto DSS was decreased due to high adsorption rate of MB molecules on the surface of ZnO-Sponge which could stop the irradiated photons of sunlight to strike with the catalytic sites offered by ZnO, consequently decreased degradation activity is observed [42]. Both the degradation efficiency and rate constant for the degradation of MB in higher concentration have revealed reduced performance of various catalyst doses of ZnO immobilized onto 1, 2 and 4 grams of DSS as shown in Supplementary (S15, 16, 17). The degradation reaction kinetics using 5, 10 and 15 mg of each sample of ZnO immobilized onto 1, 2 and 4 grams of DSS in MB concentration of 3.4×10^{-5} M in terms of measured rate constant for the simplicity is described by Supplementary (S18). Again, it indicates that the high concentration of MB is slowing down the degradation reaction kinetics. The developed ZnO immobilized onto DSS photocatalyst exhibits significant resistivity towards the use of several repeatable cycles due to proper crystal match of both ZnO and SiO_2 within the structure of sponge, thus ZnO does not lose out from the surface of DSS.

3.3. Photodegradation mechanism of MB on the surface of hybrid ZnO/DSS

The degradation mechanism is generally based on the primary oxidizing radicals produced by active radicals trapping experiment. It is believed that the dominant active oxidizing species are ($OH^{\cdot}$) followed by the electron-hole pairs then superoxide radicals generated on the irradiation of natural sunlight on the solution of MB in the presence of ZnO immobilized onto DSS. The generation of electron and hole pairs has produced high density of peroxide and hydroxyl radicals under the illumination of natural sunlight which ultimately efficiently degraded the MB as schematically shown in Figure 10. F. Mohamed *et.al.* has described that the Photodegradation process of MB completely takes in three steps with the illumination of light source [55]. Firstly, the MB molecules are adsorbed on the surface of photocatalyst and the adsorption of dye is further accelerated by the illumination of light. Secondly, the transfer of changed species takes place consisting reducing and oxidizing radicals [55]. Figure 8 shows a continuous irradiation of light with the surface of ZnO immobilized onto DSS and it creates a high density of excited electrons from the lower valence band (VB) to high energy conduction band (CB), thereby electrons and holes are produced in addition to other oxidizing radicals in the reaction system as described in Figure 8. In third step, the complete degradation of MB is either accompanied by the photogenerated electron-hole pairs or associated hydroxide radicals [56]. In our study, the ZnO immobilized onto

DSS has dual advantages offered by the photosensitivity of ZnO and the possible role of SiO_2 from sponge could not be excluded and large porosity of sponge enables the high adsorption rate in addition to oxidation of MB via created oxidizing radicals in the aqueous solution of MB and high serration out of electron hole pairs during the illumination of sunlight. It has been shown that the SiO_2 separate out the photogenerated charge carriers and provides new catalytic sites on the basis of interaction of ZnO and SiO_2 itself [51, 57, 58, 59], therefore we observed 100% degradation efficiency of MB. Furthermore, the scavengers of a particular choice enabled the identification of selected group or radical or ions during the degradation of MB, and consequently a proposed mechanism could be obtained. The scavengers study shows a significant reduction in the photodegradation of MB, therefore in this study the reaction mechanism is mainly governed by composition of hybrid material [60]. However, the produced electrons in the conduction band of ZnO were utilized to reaction with water and oxygen molecules, resulting superoxide anions as a byproduct [61].

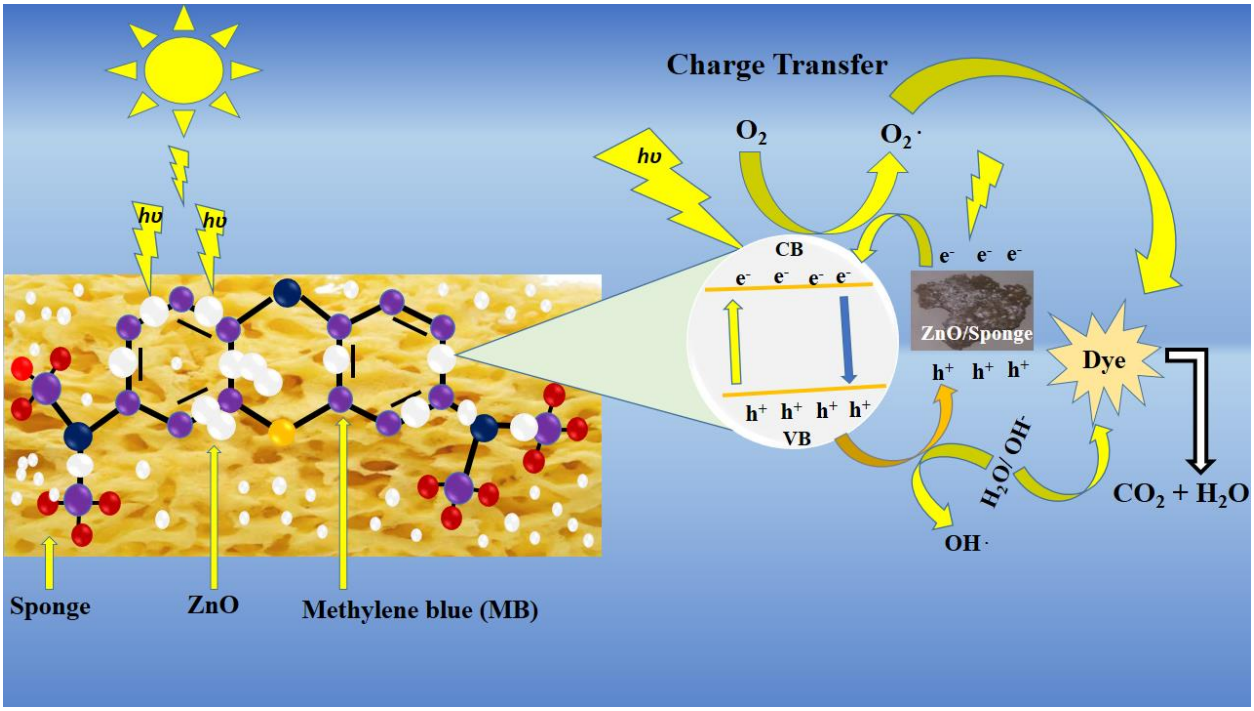

Figure 10: Proposed systematic sketch of degradation mechanism of MB on ZnO immobilized DSS floating photocatalyst in aqueous solution under illumination of natural sunlight.

The experimentally identified products during the photodegradation of MB in aqueous are reported by the published work [62] as shown in Supplementary (S19). Briefly, at the beginning the sulfur-nitrogen conjugated part of the MB chemical structure is interacting with (·OH) radicals and resulted a product of 2-amino-4-(N,N-dimethyl)-benzenesulfonic acid) at stage b and product (4-N,N-dimethyl)-aniline) at stage c. Furthermore, the some portion of stage b produces (2,4-hexadiene-1,6-diol) as a stable product. And other portion of stage b is oxidized and deaminized to (p-nitrobenzensulfonic acid) at stage d and (benzensulfonic acid) at stage e. At the stage c, the obtained product is oxidized and deaminized into (4-(N,N-dimethyl)-phenol) at stage i and (hydroquinone) at stage j. Then a portion of produced reaction intermediates at stage e and j are attacked by (·OH) radicals and resulted into unzipped products like (propionic acid) at stage j and (malonic acid) h stage. Furthermore, these products are oxidized into variety of nonhazardous mineralized products like carbon dioxide (CO_2) and water (H_2O) see the Supplementary (S19).

To investigate the repeatability and stability of 15 mg of ZnO immobilized onto 4 gram of DSS, several experiments were performed in MB concentration of 2.50×10^{-5} M under the illumination of natural sunlight as shown in Figure 11. After the run of each cycle, the ZnO immobilized photocatalyst was washed several time with the deionized water in order to verify the complete removal of adsorbed MB molecules from the surface, then it was dried followed by squeezed prior to the next photocatalytic experiment. Irrespective of careful washing of used ZnO immobilized onto DSS catalyst, the complete removal of MB from the surface of photocatalyst was not possible to achieve. Thus, the performance of presented floating photocatalyst was lost after the first cycle due to firmly bound MB molecules with the surface of ZnO immobilized DSS and blockage of illuminated photons of light resulted a no possibility of them to reach at the surface of ZnO immobilized onto sponge. After that, the ZnO immobilized onto DSS maintained the degradation performance without any abrupt loss which could be assigned to unique structural features of DSS. Another reason for the loss of performance of ZnO immobilized onto DSS during reusability test is indexed to decrease in the intensity of sunlight which enabled the less number of photons to reach at the surface of immobilized ZnO as all the recycles were done at the same day. From reusability test, it is clear that ZnO nanosheets were strongly attached with the surface of DSS due to presence of SiO_2 as crystal lattices are similar which facilitated the growth of ZnO crystal on the sponge. The performance evaluation of our fabricated ZnO/DSS floating photocatalyst is compared with recently reported excellent floating photocatalysts is given in Supplementary

Information (Table S2). The proposed material is simple, low cost, easily prepared and efficient for the removal of MB from aqueous solution under the illumination of natural sunlight can be of great consideration for practical wastewater treatment applications.

Supplementary (S20) represents the impedance spectra of pure ZnO, DSS and hybrid ZnO/DSS photocatalyst. The Nyquist plots are well characterized by fitted equivalent circuit. The prepared materials describe the semicircle arcs. The area of arcs define the charge transfer resistance as shown in Supplementary (S19). It is obvious that ZnO/DSS has verified the smallest semicircle arc compare to pure ZnO and DSS, confirming the clear indicator for the excellent performance during photodegradation process. The estimated charge transfer values for pure DSS (sample1), pristine ZnO (sample 2) and ZnO/DSS hybrid photocatalyst prepared with highest amount of DSS (sample 3) are 876 Ohms, 312 Ohms and 163 Ohms respectively.

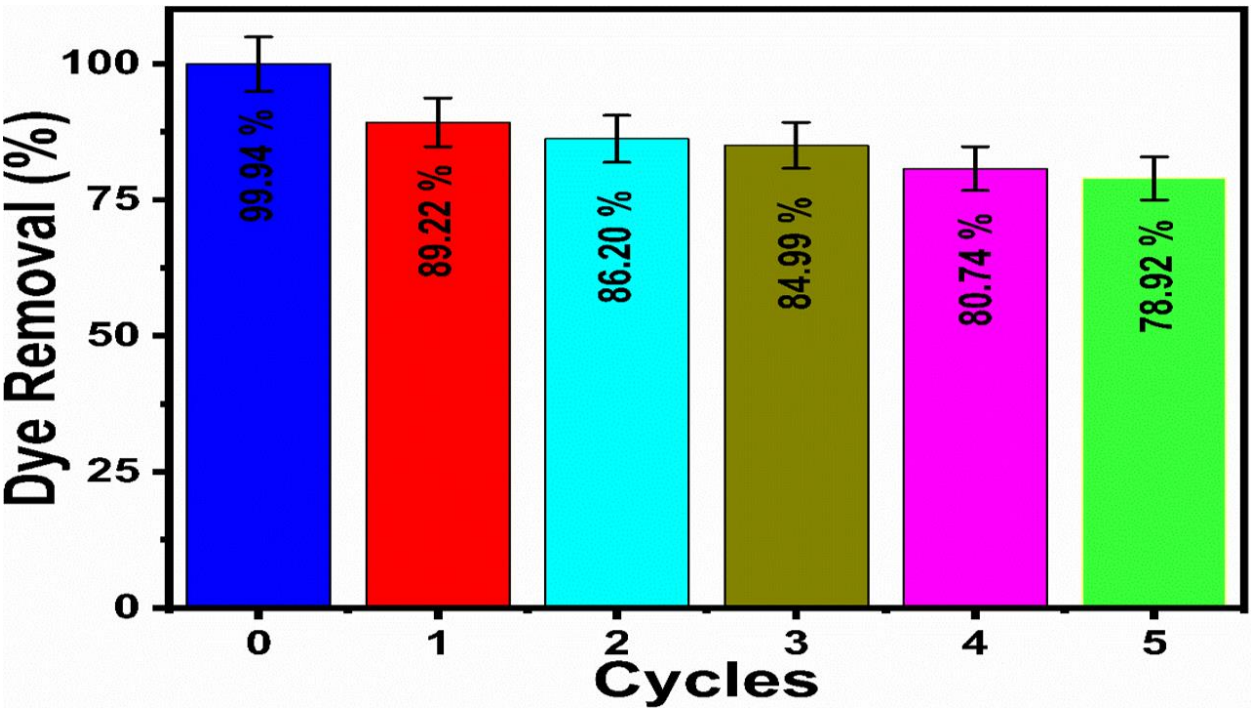

Figure 11: Reusability results for the 15 mg catalyst of ZnO immobilized onto 4 grams of DSS in MB concentration of 2.50 $\times 10^{-5}$ M for the time interval of 160 min under the illumination of sunlight

3.4. Antibacterial study of ZnO immobilized onto 1 and 4 grams of Dead Sea Sponge (DSS)

The antibacterial study of pure DSS, pure ZnO and ZnO coated sponge was analyzed by adopting the agar well diffusion method using *E.coli* and *P. areuginosa* as the medium.

Supplementary Figure (S21) shows that zone of inhibition of bacterial species growth is caused by the pure ZnO is different from the zone of inhibition occurred by ZnO immobilized onto 4 grams of DSS. Moreover, ZnO immobilized onto 4 grams of DSS samples introduce greater zone of inhibition as compared to the pure DSS and ZnO and the measurement of growth inhibition of bacterial strains are tabulated in Supplementary Table S3. Haque, et al. has described that the antibacterial activity of nanoparticles is a size dependent, as the particle size decreases, antibacterial effectiveness of particles will highly improve [63, 64]. Usually, three mechanisms were involved behind the interaction between nanoparticles and bacteria. The initial mechanism was involved the formation of active hydroxyls, second mechanism involved the deposition of nanoparticles on the bacterial surface and in the final, nanoparticles accumulates in the periplasmic zone of the bacterial cell which disorders the cellular operations and instantaneously muddled the membrane. Though, in case of E. coli, ZnO material initially muddle the cell membrane of E. coli and comes in the cytoplasmic region. Locating themselves in the cytoplasm region, the material neutralizes the respiratory enzymes and enhance the emersion of cytoplasmic contents into the outward direction which impairs the membrane and finally kills E. coli bacteria resulting in a zone of inhibition of bacterial growth around itself [65, 66]. The ZnO together with DSS has shown improved antibacterial activity and offers simultaneous effective solution of wastewater treatment and higher disinfection activity.

4. Conclusions

In this study, we have fabricated ZnO/DSS hybrid composite via hydrothermal process. This composite acts as a highly active floating photocatalyst towards approximately 100% degradation efficiency for MB in aqueous solution under the illumination of natural sunlight. The effect of catalyst dose and initial MB dye concentration were studied for various fabricated ZnO/DSS photocatalysts. Structurally, the developed photocatalyst has a high interconnected network of porous architecture which has effectively hosted thin ZnO nanosheets. Significantly, the prepared ZnO/DSS hybrid material is remarkably efficient as evident by the simultaneous high rate of adsorption and oxidation of MB under sunlight illumination. Interestingly both pristine DSS and ZnO gave poor and slow photocatalytic performance towards degradation of MB upon irradiation

with sunlight. Whereas, the immobilization of ZnO onto DSS has resulted in 100% degradation efficiency for MB in a very short time intervals leading to a high degradation rate constant of 3.351×10^{-2} min^{-1}. Additionally, ZnO/DSS composite has a natural disinfection activity during the degradation of the dye as it killed any existing pathogens, thus it does not require any additional chemical or reagent to treat the pathogens present in the treated water. Taken together, the improved degradation performance could be attributed to multi catalytic centers produced by immobilized ZnO onto favorable composition of DSS and further facilitated by the strong charge separation of electron and hole pairs. We found an optimized catalyst dose of 15 mg of ZnO immobilized onto 4 grams of DSS is facile, low cost, excellent reusability and very efficient photocatalyst with a high profile of practicality towards the solution of environmental problems especially organic dyes degradation from industrial wastewater. Hence, we believe that DSSs can be used as a host floating substrate for the wide range of photosensitive nanostructures for plenty of repeatable recycles. Also, the prepared composite could be of great interest for the wide range of adsorption processes where practical aspects are of immediate need.

Acknowledgment

We extend our sincere appreciation to the Researchers Supporting Project (RSP-2022/79) at King Saud University, Riyadh, Saudi Arabia. B.V. thank the platform “Microscopies, Microprobes and Metallography (3M)” (Institut Jean Lamour, IJL, Nancy, France) for access to SEM facilities and F. Alnjiman for his valuable help.

Author contribution

Muhammad Ali Bhatti did the photocatalytic experiment and discuss the results, Khalida faryal Almani partially supervised the work, Aneela Tahira analyzed the XRD data, Aqeel Ahmed Shah did the XRD measurement, Iftikhar Ahmed chana involved in phtocatalytic discussion, Umair Aftab participated in the FTIR experiment, Mazhar Hussain Ibupoto did the EDS analysis, Abdul Nabi Mirjat did the antibacterial measurement, Amal Aboelmaaref analyzed the trapping experiment, Ayman Nafady edited the draft and partially supported the work, Brigitte, Vigolo analyzed the SEM and edited the draft of manuscript, Zafar Hussain Ibupoto, conceptualized the work, supervised, and wrote first draft of manuscript. Finally all authors agreed for the submission.

Conflict of interest statement

Authors declare there are not conflict of interest in this research work

5. References

[1]. Subki NS 2017 Environmental contamination by batik wastewater and the potential application of activated carbon from pineapple waste for wastewater treatment. *University Sains Malaysia*.

[2]. Zhang X, Yin Y, Sun Z, Du Y, Ma S and Wu Y 2016 Cr/S/TiO2-loaded hollow glass microspheres as an efficient and recyclable catalyst for the photocatalytic degradation of indigo carmine under visible light *Quim. Nova.* **39** 956– 961.

[3]. Gao T and Wang T 2021 Preparation of Ag2O/TiO2 nanocomposites by two-step method and study of its degradation of RHB *J. Mol. Struct.* **1224** 129049.

[4]. Wu Y, Pang H, Liu Y, Wang X, Yu S, Fu D, Chen J X and Wang X 2019 Environmental remediation of heavy metal ions by novel-nanomaterials: a review *Environmental pollution*. **246** 608-620.

[5]. Li W, Zuo Y, Jiang L, Yao D, Chen Z, He G and Chen H 2020 Bi2Ti2O7/TiO2/RGO composite for the simulated sunlight-driven photocatalytic degradation of ciprofloxacin *Materials Chemistry and Physics*. **256** 123650.

[6]. An Y, Zheng P and Ma X 2019 Preparation and visible-light photocatalytic properties of the floating hollow glass microspheres–TiO 2/Ag 3 PO 4 composites *RSC Adv.* **9** 721-729.

[7]. Derikvandi H and Nezamzadeh-Ejhieh A 2017 Increased photocatalytic activity of NiO and ZnO in photodegradation of a model drug aqueous solution: effect of coupling, supporting, particles size and calcination temperature *J. Hazard. Mater.* **321** 629– 638.

[8]. Li B, Hao Y, Zhang B, Shao X and Hu L 2017 A multifunctional noble-metal-free catalyst of CuO/TiO2 hybrid nanofibers *Appl. Catal. A.* **531** 1– 12.

[9]. Bai X, Wang L, Zong R, Lv Y, Sun Y and Zhu Y 2013 Performance enhancement of ZnO photocatalyst via synergic effect of surface oxygen defect and graphene hybridization *Langmuir*. **29** 3097–3105.

[10]. Ong CB, Ng LY and Mohammad AW 2018 A review of ZnO nanoparticles as solar photocatalysts: Synthesis, mechanisms and applications *Sustain. Energy Rev*. **81** 536–551.

[11]. Xue X, Zang W, Deng P, Wang Q, Xing L, Zhang Y and Wang ZL 2015 Piezo-potential enhanced photocatalytic degradation of organic dye using ZnO nanowires *Nano Energy Nano Environ.* **13** 414–422.

[12]. Pirhashemi M and Habibi-Yangjeh A 2018 Facile fabrication of novel ZnO/CoMoO4 nanocomposites: Highly efficient visible-light-responsive photocatalysts in degradations of different contaminants *J. Photochem. Photobiol. Chem*. **363** 31–43.

[13]. Abdolhoseinzadeh A and Sheibani S 2020 Enhanced photocatalytic performance of Cu2O nano-photocatalyst powder modified by ball milling and ZnO *Adv. Powder Technol.* **31** 40–50.

[14]. Hir ZAM, Moradihamedani P, Abdullah AH and Mohamed MA 2017 Immobilization of TiO2 into polyethersulfone matrix as hybrid film photocatalyst for effective degradation of methyl orange dye *Mater. Sci. Semicond. Process.* **57** 157–165.

[15]. Choi H, Stathatos E and Dionysiou DD 2007 Photocatalytic TiO2 films and membranes for the development of efficient wastewater treatment and reuse systems *Desalination*. **202** 199–206.

[16]. Lopez L, Daoud WA, Dutta D, Panther BC and Turney TW 2013 Effect of substrate on surface morphology and photocatalysis of large-scale TiO2 films *Appl. Surf. Sci*. **265** 162–168.

[17]. Srikanth B, Goutham R, Badri Narayan R, Ramprasath A, Gopinath KP and Sankaranarayanan AR 2017 Recent advancements in supporting materials for immobilised photocatalytic applications in waste water treatment *J. Environ. Manag.* **200** 60–78.

[18]. Hossain S, Chu W-S, Lee CS, Ahn S-H and Chun D-M 2019 Photocatalytic performance of few-layer Graphene/WO3 thin films prepared by a nano-particle deposition system *Mater. Chem. Phys*. **226** 141-150.

[19]. Grbić B, Radić N, Stojadinović S, Vasilić R, Dohčević-Mitrović Z, Šaponjić Z and Stefanov P 2014 TiO2/WO3 photocatalytic composite coatings prepared by spray pyrolysis *Surf. Coating. Technol*. **258** 763–771.

[20]. Di Mauro A, Cantarella M, Nicotra G, Pellegrino G, Gulino A, Brundo MV, Privitera V and Impellizzeri G 2017 Novel synthesis of ZnO/PMMA nanocomposites for photocatalytic applications *Sci. Rep.* **7** 40895.

[21]. Singh S, Mahalingam H and Singh PK 2013 Polymer-supported titanium dioxide photocatalysts for environmental remediation: A review. *Applied Catalysis A: General*, **462** 178-195.

[22]. Masimukku S, Hu YC, Lin ZH, Chan SW, Chou TM and Wu JM 2018 High efficient degradation of dye molecules by PDMS embedded abundant single-layer tungsten disulfide and their antibacterial performance *Nano Energy Nano Environ.* **46** 338–346.

[23]. Liu J, Ye L, Wooh S, Kappl M, Steffen W and Butt HJ 2019 ptimizing hydrophobicity and photocatalytic activity of PDMS-coated titanium dioxide *ACS Appl. Mater. Interfaces*. **11** 27422–27425.

[24]. Hickman R, Walker E and Chowdhury S 2018 TiO2-PDMS composite sponge for adsorption and solar mediated photodegradation of dye pollutants *J. Water Process Eng*. **24** 74–82.

[25]. Qiu S, Bi H, Hu X, Wu M, Li Y and Sun L 2017 Moldable clay-like unit for synthesis of highly elastic polydimethylsiloxane sponge with nanofiller modification *RSC Adv.* **7** 10479–10486.

[26]. Jang S and Oh JH 2018 Rapid fabrication of microporous batio 3/pdms nanocomposites for triboelectric nanogenerators through one-step microwave irradiation *Scientific reports*. **8** 1-9.

[27]. Mark JE 2004 Some interesting things about polysiloxanes *Acc. Chem. Res.* **37** 946–953.

[28]. Lamberti A 2015 Microfluidic photocatalytic device exploiting PDMS/TiO2 nanocomposite *Appl. Surf. Sci*. **335** 50–54.

[29]. Santiago AAG, Gondim JGS, Tranquilin RL, Silva FS, Fernandez FF, Costa MC B, Motta FV and Bomio MRD 2020 Development of ZnO/PDMS nanocomposite with photocatalytic/hydrophobic multifunction *Chem. Phys. Lett.* **740** 137051.

[30]. Saddam H and Chun DM 2020 ZnO decorated polydimethylsiloxane sponges as photocatalysts for effective removal of methylene blue dye *Materials Chemistry and Physics.* **255** 123589.

[31]. Elashmawi IS and Gaabour LH 2015 Raman, morphology and electrical behavior of nanocomposites based on PEO/PVDF with multi-walled carbon nanotubes *Results Phys.* **5** 105– 110.

[32]. Jing L, Zhou W, Tian G and Fu H 2013 Surface tuning for oxide-based nanomaterials as efficient photocatalysts.*Chem. Soc. Rev.* **42** 9509.

[33]. Zhang L, Xing Z, Zhang H, Li Z, Zhang X, Zhang Y, Li L and Zhou W 2014 Multifunctional floating titania-coated macro/mesoporous photocatalyst for efficient contaminant removal *ChemPlusChem.* **80** 623– 629.

[34]. Anghel D, Lascu A, Epuran C, Fratilescu I, Ianasi C, Birdeanu M and Fagadar-Cosma E 2020 Hybrid materials based on silica matrices impregnated with pt-porphyrin or ptnps destined for CO2 gas detection or for wastewaters color removal *Int. J. Mol. Sci.* **21** 4262.

[35]. Wan JM, Wu ZZ, Wang HG and Zheng XM 2012 Visible-light photocatalytic degradation of methylene blue with porphyrin-sensitized TiO2 *Adv. Mater. Res.* **441** 544–548.

[36]. Gholamrezapor E and Eslami A 2019 Sensitization of magnetic TiO 2 with copper (II) tetrahydroxylphenyl porphyrin for photodegradation of methylene blue by visible LED light *J. Mater. Sci. Mater. Electron.* **30** 4705–4715.

[37]. https://www.naturalfrenchsoap.com/blog/7-surprising-ways-youll-benefit-from-using-natural-sponges

[38]. Thandavan TM, Gani SM, Wong CS and Nor RM 2015 Evaluation of Williamson–Hall strain and stress distribution in ZnO nanowires prepared using aliphatic alcohol. Journal of Nondestructive Evaluation. **34** 1-9.

[39]. Reddy DA, Ma R and Kim TK 2015 Efficient photocatalytic degradation of methylene blue by heterostructured ZnO–RGO/RuO2 nanocomposite under the simulated sunlight irradiation *Ceramics International*, **41** 6999-7009.

[40]. Xiong HM, Shchukin DG, Möhwald H, Xu Y and Xia YY 2009 Sonochemical synthesis of highly luminescent zinc oxide nanoparticles doped with magnesium (II). Angewandte Chemie International Edition. **48** 2727-31.

[41]. Rezaei-Zarchi S, Javed A, Mirjalili H, Abarghouei HB and Hashemizadeh SA 2009 Characterization and electrochemical study of nano-composition based methylene blue- and riboflavin-nafion on the surface of gold electrode *Turkish Journal of Chemistry*. **33** 411-420.

[42]. Wang F, Li C and Yu JC 2012 Hexagonal tungsten trioxide nanorods as a rapid adsorbent for methylene blue *Sep. Purif. Technol.* **91** 103–107.

[43]. Duran A, Serna C, Fornes V and Navarro JMF 1986 Structural considerations about SiO2 glasses prepared by sol-gel Non-Cryst. Solids, **82** 69–77.

[44]. Bertoluzza A, Fagnano C, Morelli MA, Gottardi V and Guglielmi M 1982 Raman and infrared spectra on silica gel evolving toward glass *J. NonCryst Solids*. **48** 117–128

[45]. Gopal KV, Narasimhulu J and Rao L 2004 *Acta, Part A*. **60** 2441– 2448.

[46]. Galedari NA, Rahmani M and Tasbihi M 2017 Preparation, characterization, and application of ZnO@ SiO 2 core–shell structured catalyst for photocatalytic degradation of phenol *Environ. Sci. Pollut. Res*. **24** 12655–12663.

[47]. Aly HF and Abd-Elhamid AI 2018 Photocatalytic degradation of methylene blue dye using silica oxide nanoparticles as a catalyst *Water Environ Res*. **90** 807-817.

[48]. Zhong JB, Li JZ, He XY, Zeng J, Lu Y, He JJ and Zhong F 2014 Fabrication and catalytic performance of SiO2-ZnO composite photocatalyst *Synth. React. Inorganic, Met. Nano-Metal Chem*. **44** 1203-1207.

[49]. Patil SP, Patil RP, Mahajan VK, Sonawane GH, Shrivastava VS and Sonawane SH 2016 Facile sonochemical synthesis of BiOBr-graphene oxide nanocomposite with enhanced photocatalytic activity for the degradation of Direct green *Mater Sci Semicond Process*. **52** 55–61.

[50]. Chu CY and Huang MH 2017 Facet-dependent photocatalytic properties of Cu 2 O crystals probed by using electron, hole and radical scavengers *J Mater Chem. A.* **5** 15116–15123.

[51]. Li S, in Q, Liu X, Yang L, Ding J, Dong F, Li Y, Irfan M and Zhang P 2018 Fast photocatalytic degradation of dyes using low-power laser-fabricated Cu 2 O–Cu nanocomposites *RSC Adv*. **8** 20277–20286.

[52]. Sunil G. S, Vilas K. M, Sandip P. P, and Gunvant H. S 2020 Effect of doping parameters on photocatalytic degradation of methylene blue using Ag doped ZnO nanocatalyst, SN Applied Sciences. **2** 820

[53]. Mondol. B, Sarker. A, Shareque.A.M, Dey.S.C, Islam. M.T, Das. A. K, Shamsuddin. S.M, Molla. M.A.I, Sarker. M 2021 Preparation of Activated Carbon/TiO2 Nanohybrids for Photodegradation of Reactive Red-35 Dye Using Sunlight. Photochem. **1** 54–6

[54]. Molla.M.A.I, Tateishi.I, Furukawa. M. Katsumata. H, Suzuki. T, Kaneco. S, 2017 Evaluation of Reaction Mechanism for Photocatalytic Degradation of Dye with Self-Sensitized TiO2 under Visible Light Irradiation. Open J. Inorg. Non-Met. Mater.**7** 1–7.

[55]. Mohamed F, Abukhadra MR and Shaban M 2018 Removal of safranin dye from water using polypyrrole nanofiber/Zn-Fe layered double hydroxide nanocomposite (Ppy NF/Zn-Fe LDH) of enhanced adsorption and photocatalytic properties *Sci. Total Environ.* **640** 352-363.

[56]. Lan Y, Lu Y and Ren Z 2013 Mini review on photocatalysis of titanium dioxide nanoparticles and their solar applications *Nano Energy*. **2** 1031-1045.

[57]. Romolini G, Gambucci M, Ricciarelli D, Tarpani L, Zampini G and Latterini L 2021 Photocatalytic activity of silica and silica-silver nanocolloids based on photo-induced formation of reactive oxygen species. Photochemical & Photobiological Sciences. **20** 1161-72.

[58]. Tarpani L, Ruhlandt D, Latterini L, Haehnel D, Gregor I, Enderlein J and Chizhik AI 2016 Photoactivation of luminescent centers in single SiO2 nanoparticles. Nano Letters. **16** 4312-6.

[59]. Zhou W and Fu H 2018 Defect-mediated electron–hole separation in semiconductor photocatalysis. Inorganic Chemistry Frontiers. **5** 1240-54.

[60]. Astašauskas V, Bellissimo A, Kuksa P, Tomastik C, Kalbe H and Werner WS Optical and electronic properties of amorphous silicon dioxide by single and double electron spectroscopy *Journal of Electron Spectroscopy and Related Phenomena.* **241** 146829.

[61]. Chang YC and Wu SH 2020 Bi-functional Al-doped ZnO@ SnO2 heteronanowires as efficient substrates for improving photocatalytic and SERS performance. *J. Ind. Eng. Chem.* **76** (2019), pp.333–343.

[62]. Lin J, Luo Z, Liu J and Li P 2018 Photocatalytic degradation of methylene blue in aqueous solution by using ZnO-SnO2 nanocomposites *Materials Science in Semiconductor Processing*. **87** 24-31.

[63]. Haque MJ, Bellah MM, Hassan MR and Rahman S 2020 Synthesis of ZnO nanoparticles by two different methods & comparison of their structural, antibacterial, photocatalytic and optical properties *Nano Express*. **1** 010007.

[64]. Khan SA, Noreen F, Kanwal S, Iqbal A and Hussain G 2018 Green synthesis of ZnO and Cu-doped ZnO nanoparticles from leaf extracts of Abutilon indicum, Clerodendrum infortunatum, Clerodendrum inerme and investigation of their biological and photocatalytic activities *Materials Science and Engineering: C*. **82** 46-59.

[65]. Kairyte K, Kadys A and Luksiene Z 2013 Antibacterial and antifungal activity of photoactivated ZnO nanoparticles in suspension *Journal of Photochemistry and Photobiology B: Biology*. **128** 78-84.

[66]. Raghupathi KR, Ranjit TK and Adhar C M 2011 Size-dependent bacterial growth inhibition and mechanism of antibacterial activity of zinc oxide nanoparticles *Langmuir*. **27**, 4020-4028.

Supplementary Information

Renewable and eco-friendly ZnO immobilized onto Dead Sea Sponge floating materials with dual practical aspects for robotic photocatalysis and disinfection applications

Muhammad Ali Bhatti[a], Khalida Faryal Almani[a], Aqeel Ahmed Shah[g], Aneela Tahira[b], Iftkhar Ahmed Chana[g], Umair Aftab[c], Mazhar Hussain Ibupoto[e], Abdul Nabi Mirjat[f], Amal Aboelmaare[i], AymanNafady[h], Brigitte Vigolo[d], Zafar Hussain Ibupoto[b*]

[a]Institute of Environmental Sciences, University of Sindh Jamshoro, 76080, Sindh Pakistan

[b]Dr. M.A Kazi Institute of Chemistry University of Sindh Jamshoro, 76080, Sindh Pakistan

[c]Mehran University of Engineering and Technology, 7680 Jamshoro, Sindh Pakistan

[d]Université de Lorraine, CNRS, IJL, F-54000 Nancy, France

[e]Department of Zoology, Shah Abdul Latif University Khairpur Mirs

[f]Institute of Microbiology, University of Sindh Jamshoro, 76080, Sindh Pakistan

[g]Department of Metallurgy, NED university of Engineering and Technology, Karachi Pakistan

[h]Department of Chemistry, College of Science, King Saud University, Riyadh 11451, Saudi Arabia

[i]Department of Chemistry, Faculty of Science, Helwan University, Ain Helwan, Egypt

***Corresponding authors** : Zafar Hussain Ibupoto& Aneela Tahira

Email: zaffar.ibhupoto@usindh.edu.pk; aneelatahira80@gmail.com

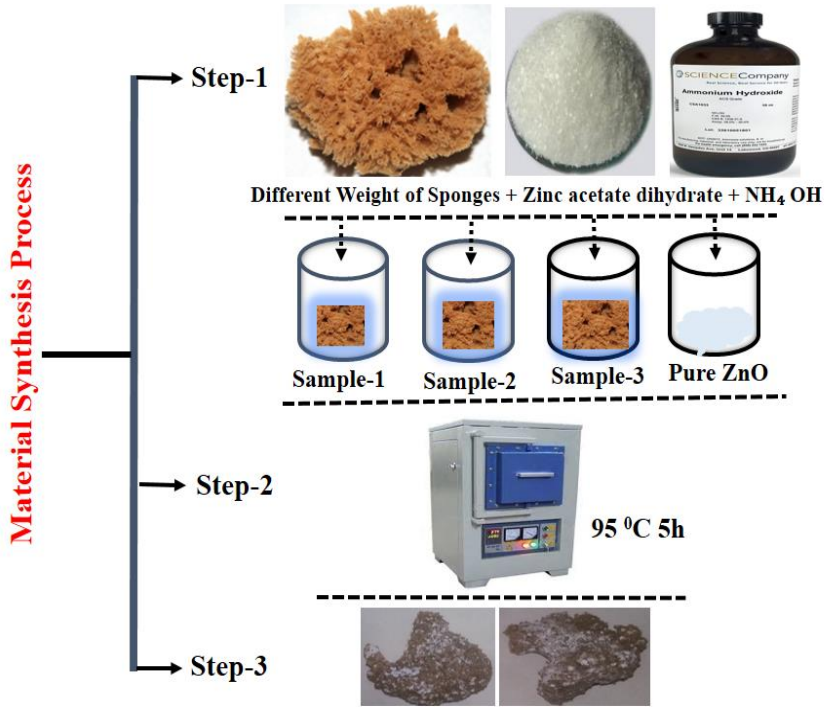

S1: Schematic diagram for the synthesis of ZnO immobilized onto gram of DSS

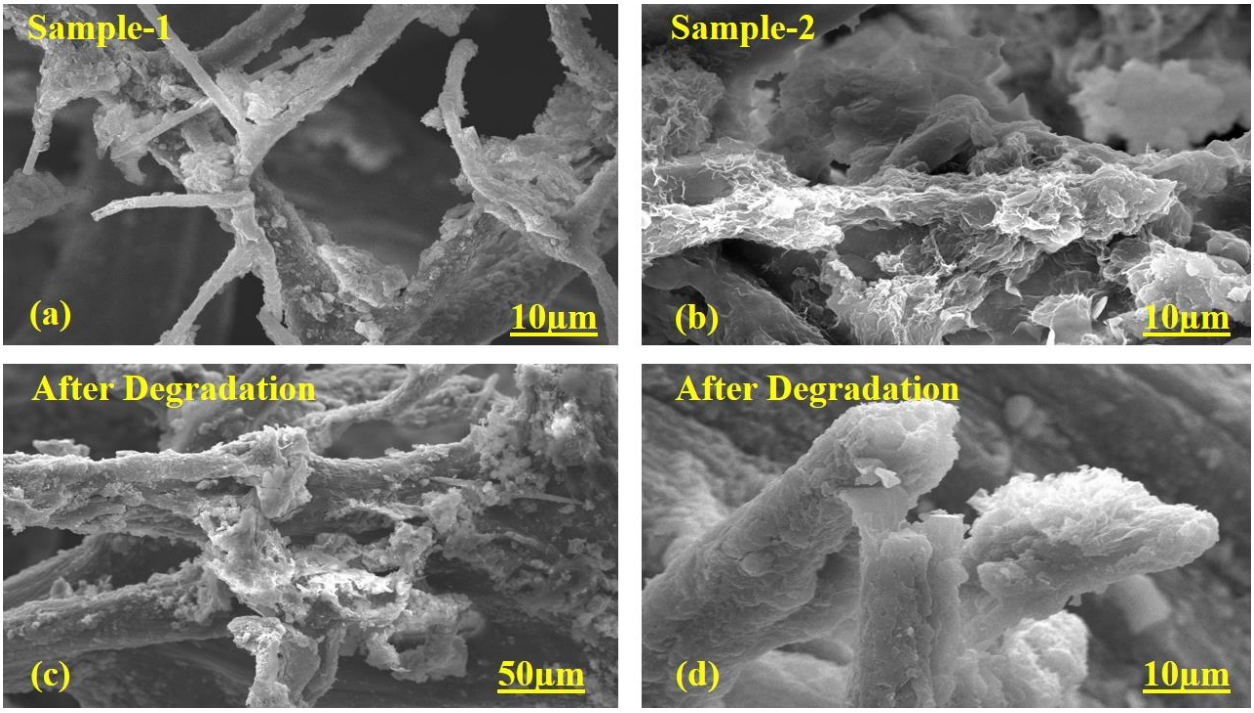

S2: SEM images of ZnO immobilized onto (a) 1 gram of DSS, (b) 2 grams of DSS, (c-d) SEM images of ZnO immobilized after the MB degradation process

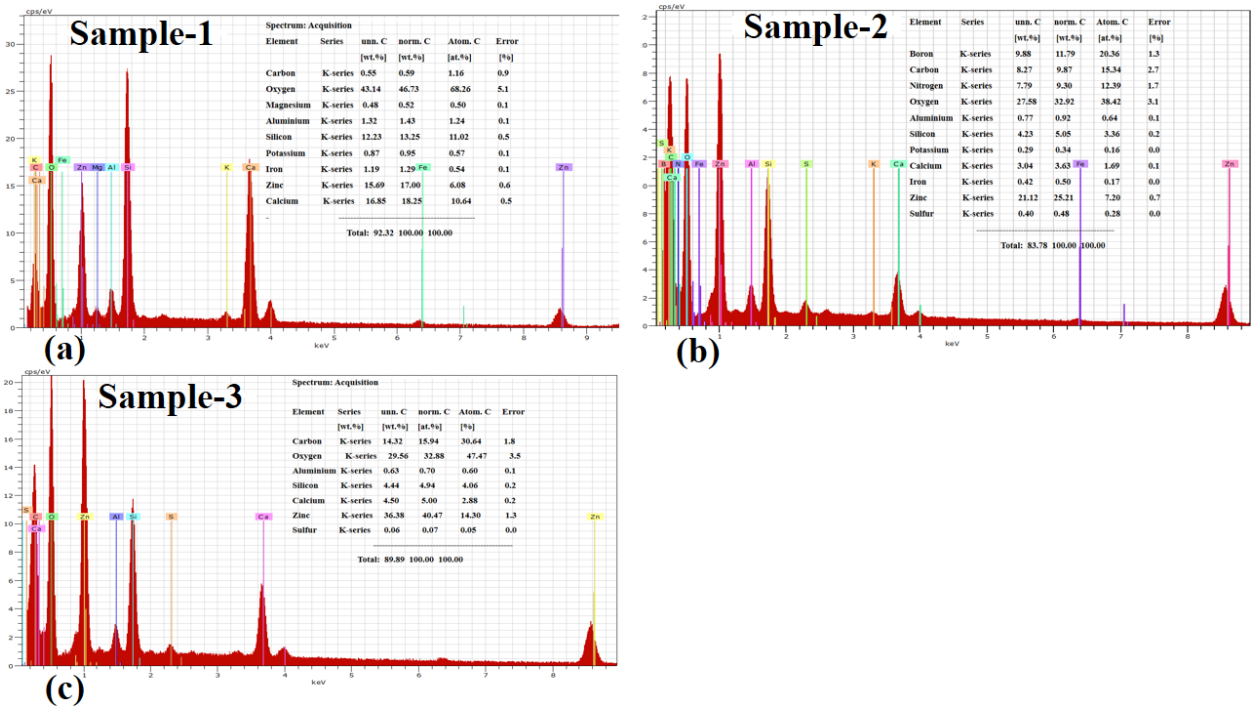

S3: EDS spectra (a) ZnO immobilized onto gram of DSS, (b) ZnO immobilized onto 2 a grams of DSS, ZnO immobilized onto 4 grams of DSS

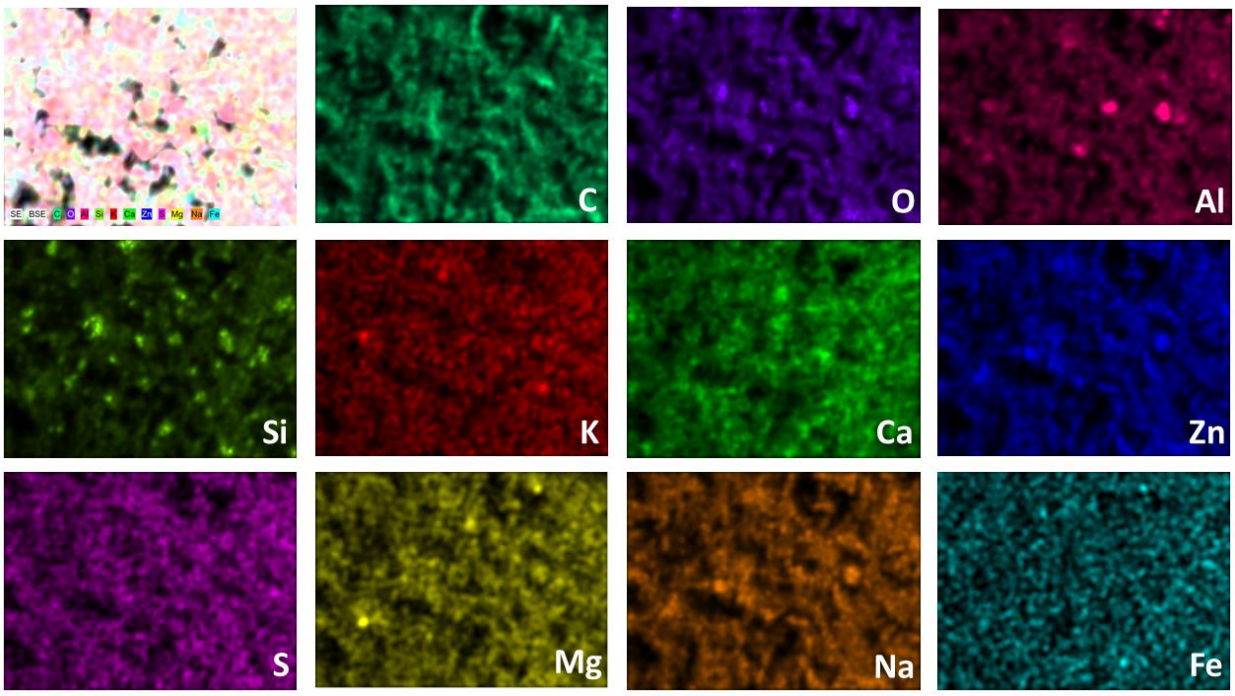

S4: EDS mapping of ZnO/DSS hybrid system containing the highest amount of DSS

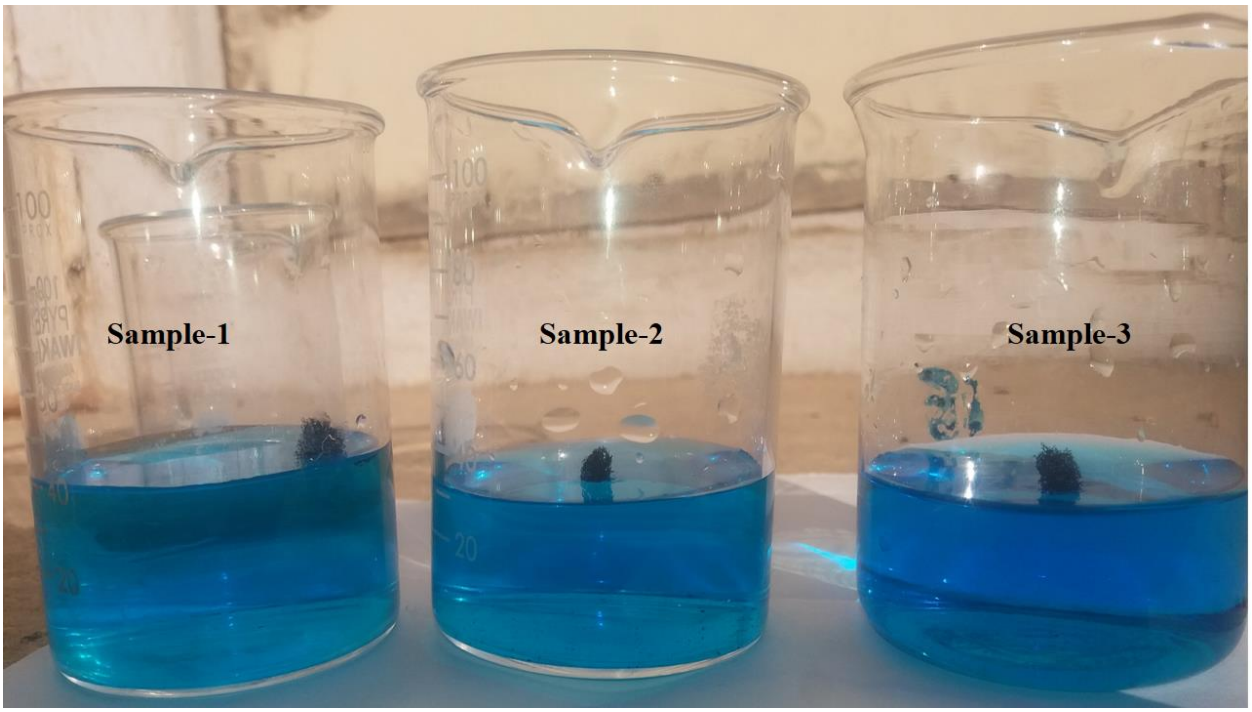

S 5**:** Digital view of 15 mg ZnO immobilized onto 1, 2 and 4 grams of DSS concentration of 2.50 $\times 10^{-5}$ M.

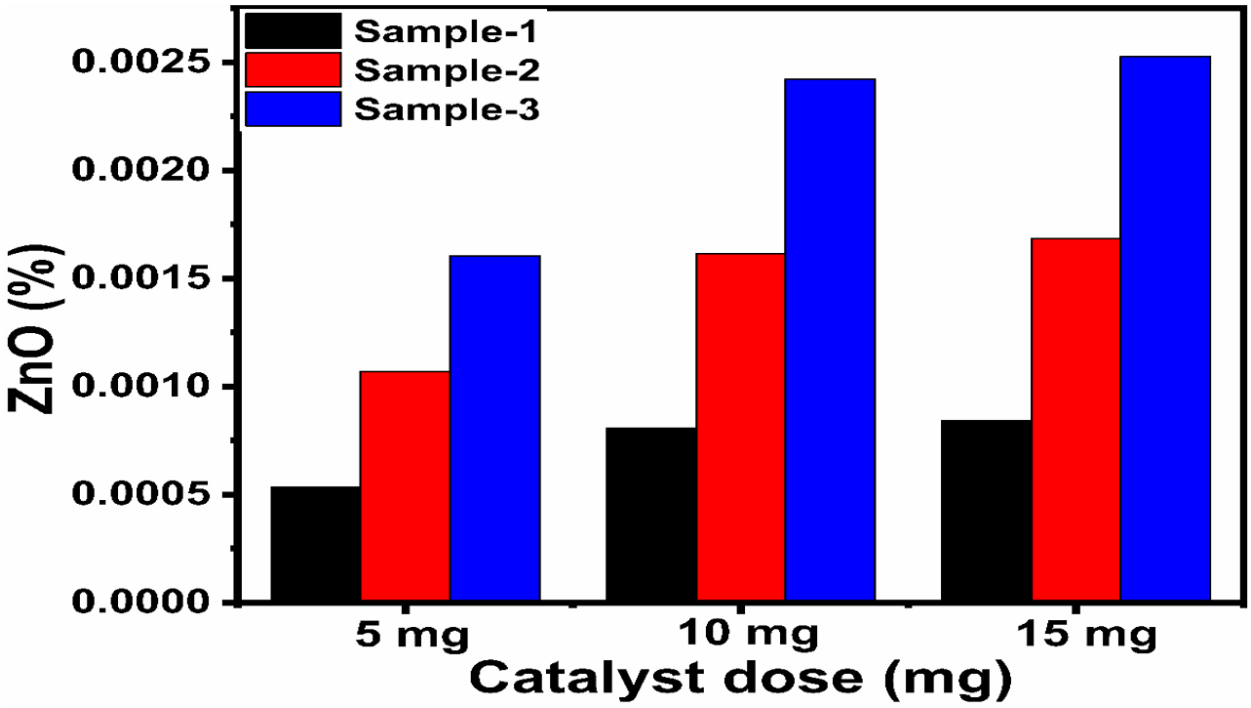

S6: shows the ZnO content present in 5, 10 and 15 mg catalyst dose of ZnO immobilized onto 1, 2 and 4 grams of DSS

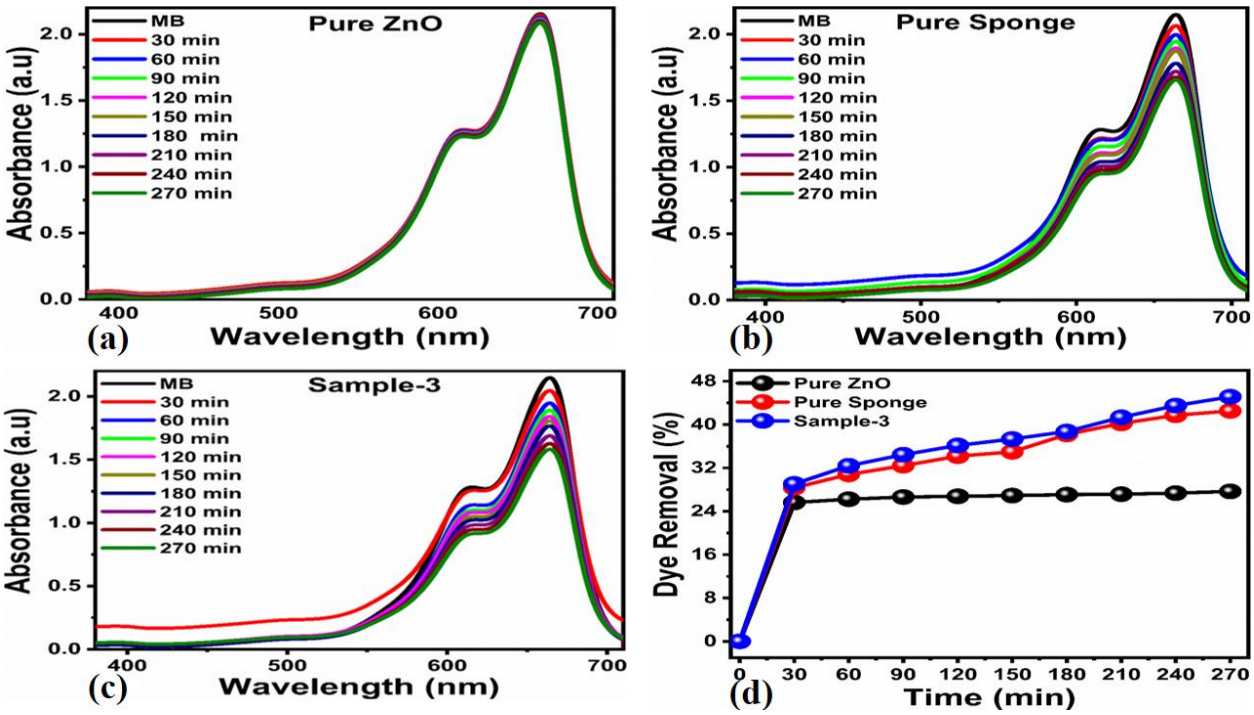

S7: (a) UV-visible absorbance spectra (a) 15 mg of pure ZnO, (b) 15 mg of pure DSS, (c) 15 mg of ZnO immobilized onto 4 grams of DSS (d) their corresponding degradation efficiency

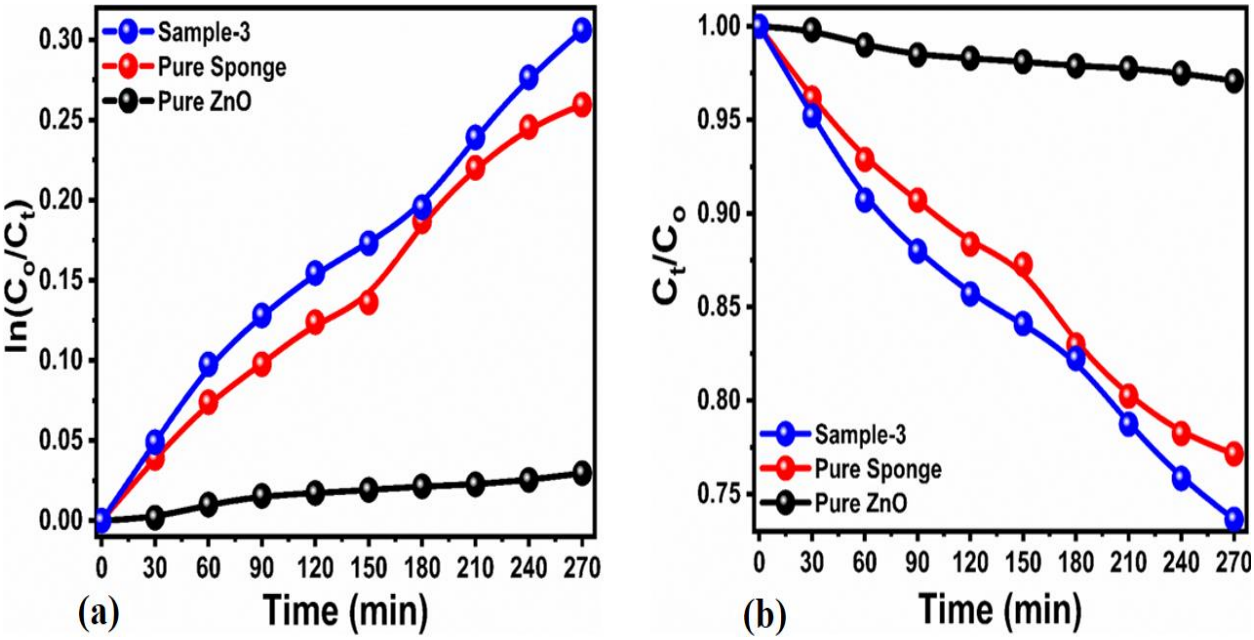

S 8: (a) Linear plotting for kinetic versus different time intervals in MB concentration of 2.50 $\times 10^{-5}$ M for the time interval of 270 min 15 mg of pure ZnO, and 15 mg of pure Dead Sea and 15 mg of ZnO immobilized onto 4 grams of DSS, (b) Reaction profile for 15 mg of pure ZnO, and

15 mg of pure DSS and 15 mg of ZnO immobilized onto DSS in MB concentration of 2.50 ×10^{-5} M for the time interval of 270 min

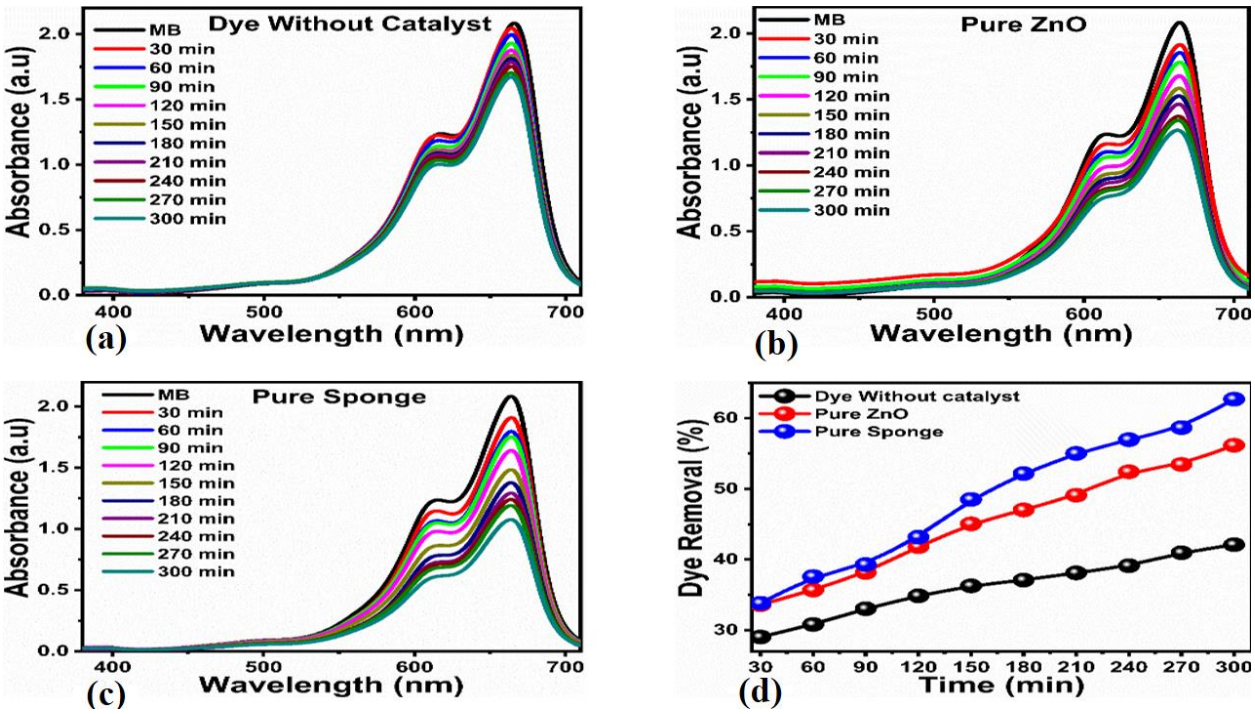

S9**:** (a) UV-visible absorbance spectra (a) MB concentration of 2.50 ×10^{-5} M under the illumination of natural sunlight without catalyst, (b) 15 mg of pure ZnO, (c) 15 mg of pure DSS, (d) their corresponding degradation efficiency

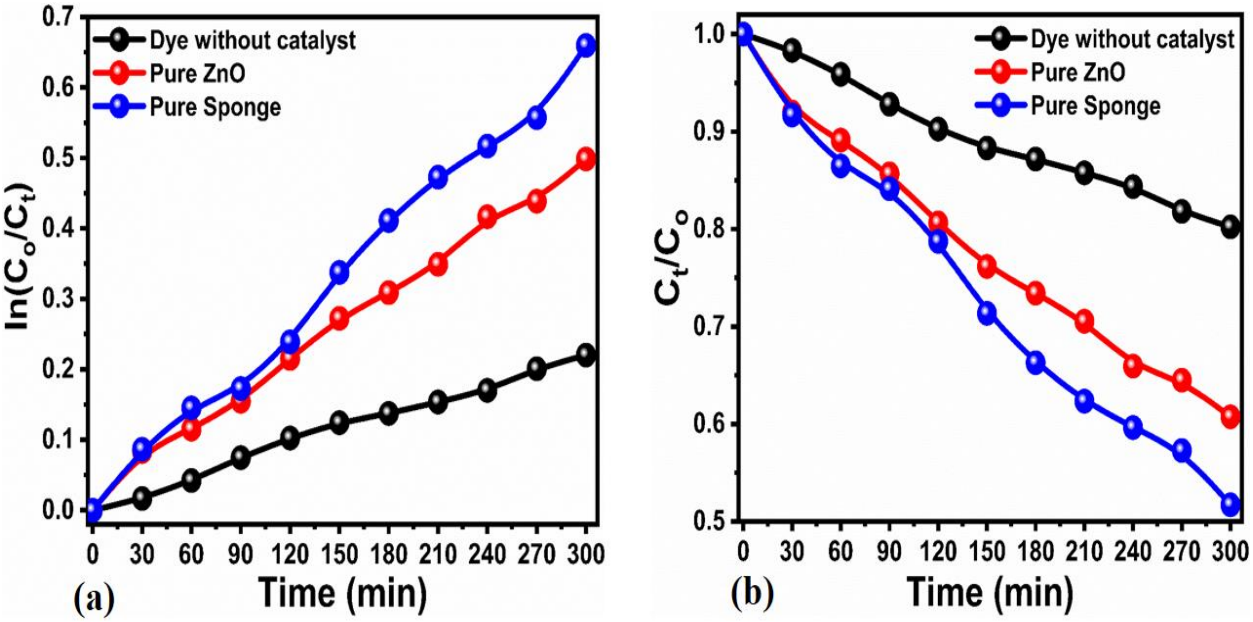

S10: (a) Linear plotting for kinetic versus different time intervals in MB concentration of 2.50 $\times 10^{-5}$ M for the time interval of 300mnuites without catalyst, 15 mg of pure ZnO, and 15 mg of pure DSS, (b) Reaction profile for dye without catalyst, 15 mg of pure ZnO, and 15 mg of pure DSS in MB concentration of 2.50 $\times 10^{-5}$ M for the time interval of 300 min.

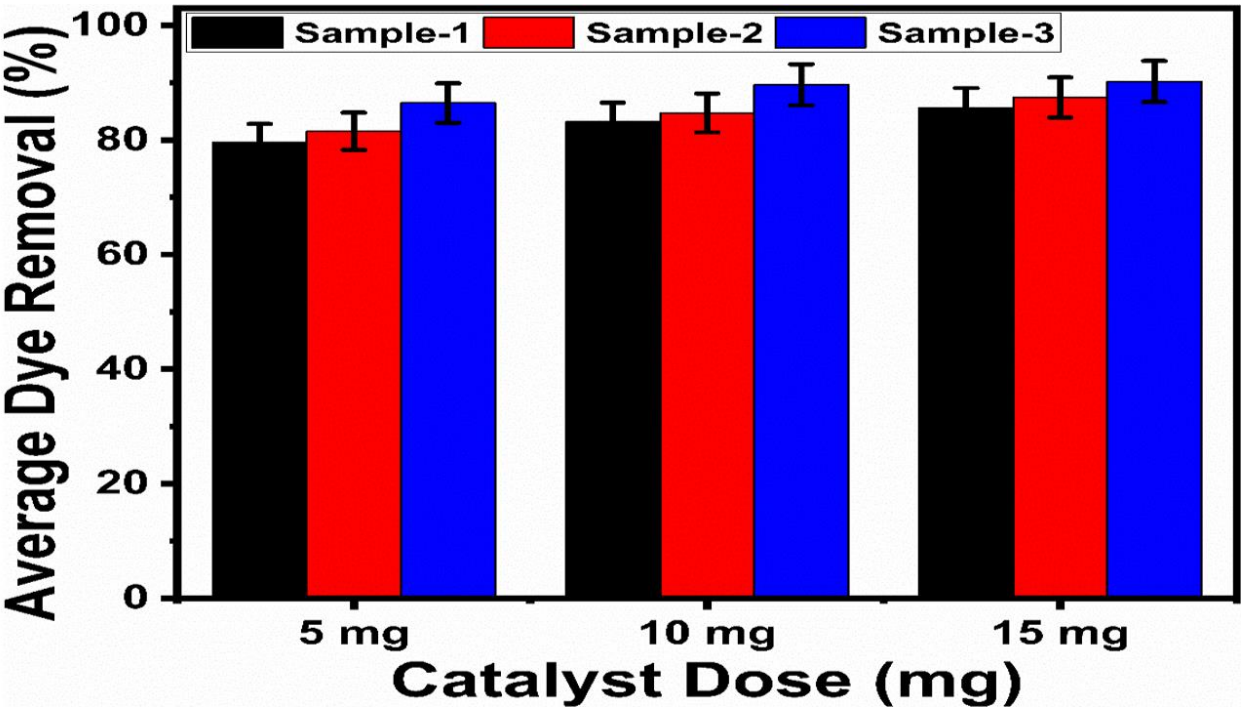

S11: Triplicate of sample 1, 2 and 4 average degradation efficiency values with error bars

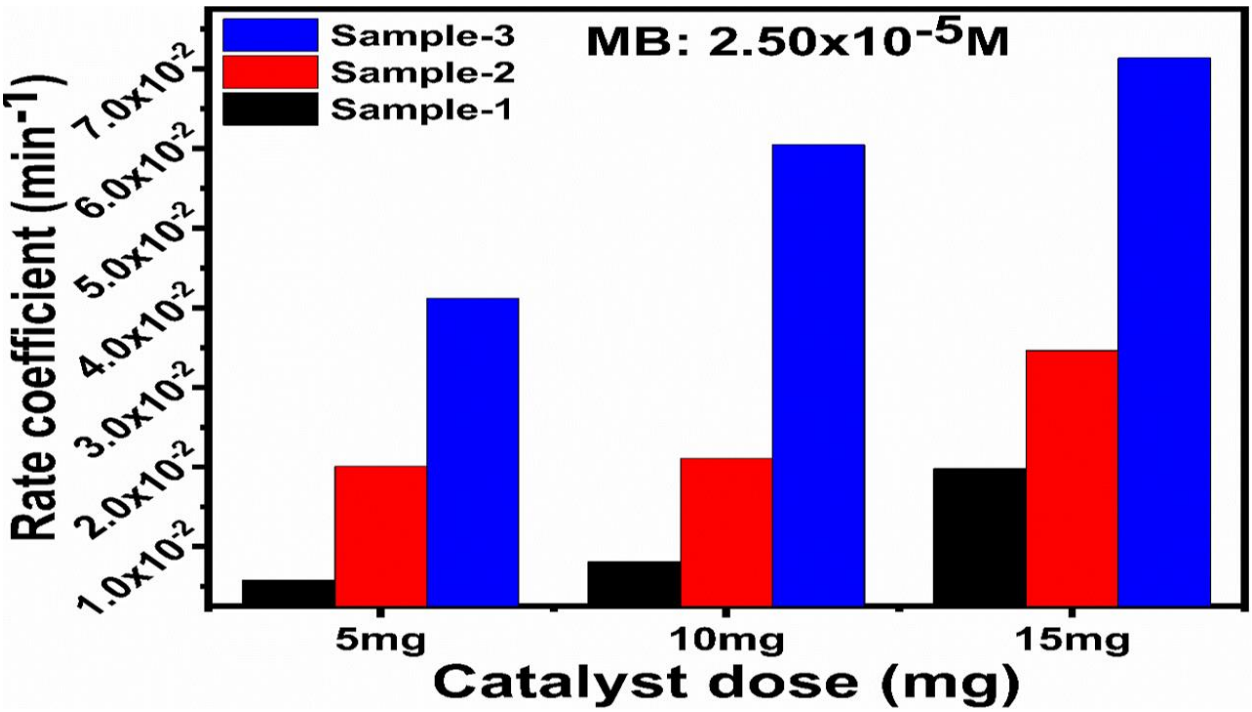

S12: Pictorial presentation of rate constants for the 5, 10 and 15 mg catalyst dose of each ZnO immobilized onto 1, 2 and 4 grams of DSS in in MB concentration of 2.50 $\times 10^{-5}$ M for the time interval of 160 min.

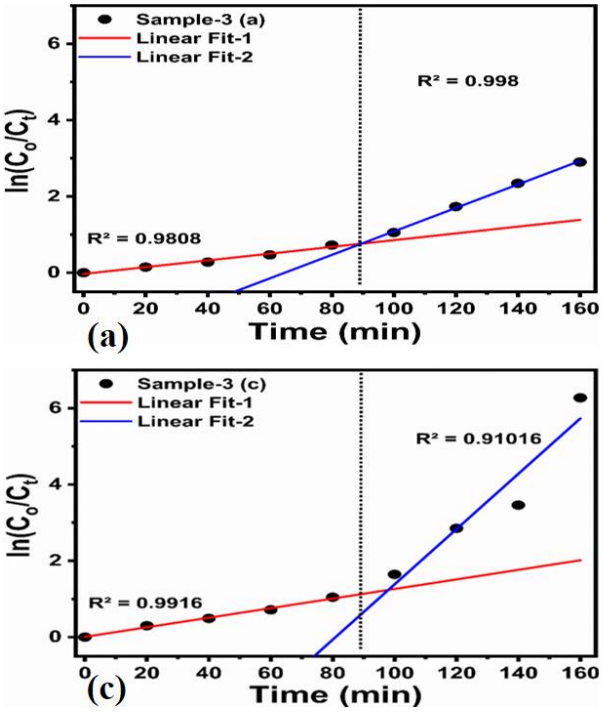

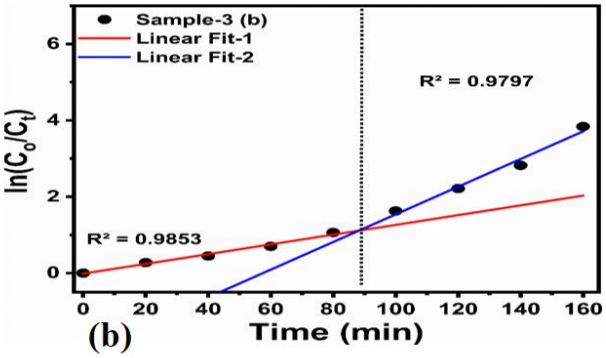

S13: plot $\ln(C_t/C_0)$ for the recalculation of rate constant of MB onto sample-3

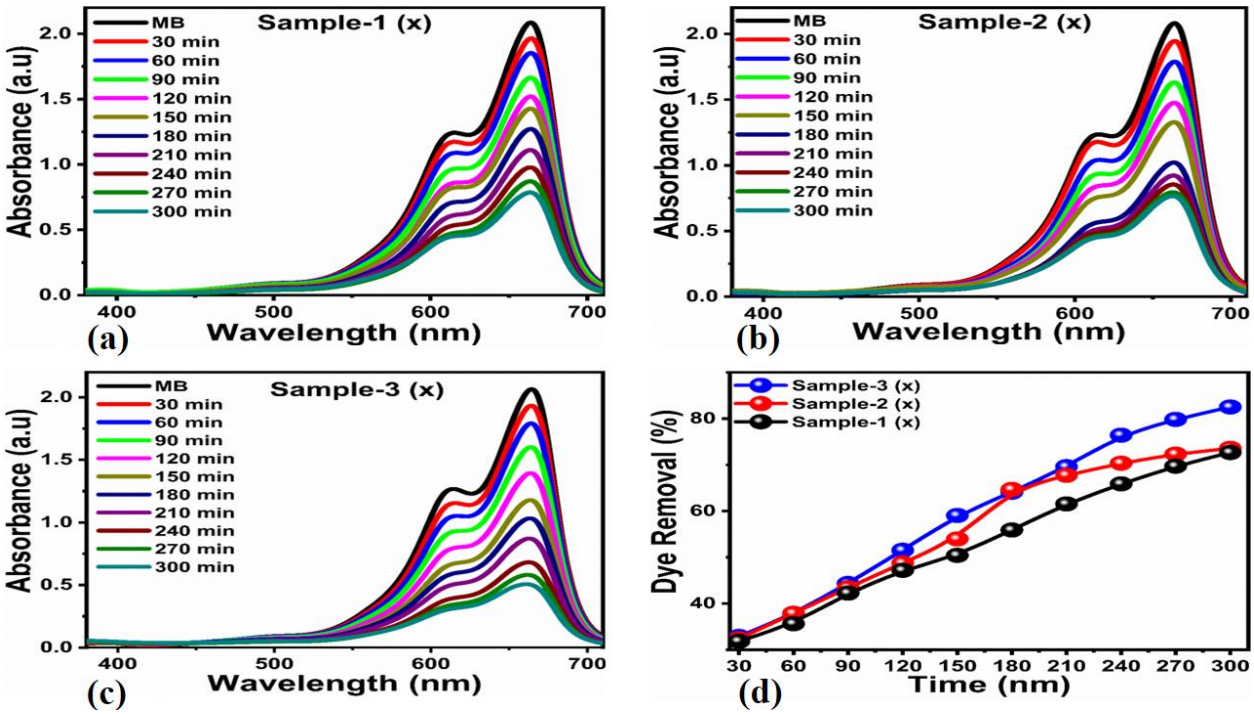

S14: UV-visible absorbance spectra in MB concentration of 3.4 $\times 10^{-5}$ M for the time interval of 300 mnuites under the illumination of natural sunlight (a) 10 mg catalyst dose ZnO immobilized onto 1 gram of DSS, (b) 10 mg catalyst dose ZnO immobilized onto 2 gram of DSS, (c) 10 mg catalyst dose ZnO immobilized onto 4 gram of DSS, (d) Degradation efficiency of 10 mg catalyst dose ZnO immobilized onto 1, 2 and 4 grams of DSS

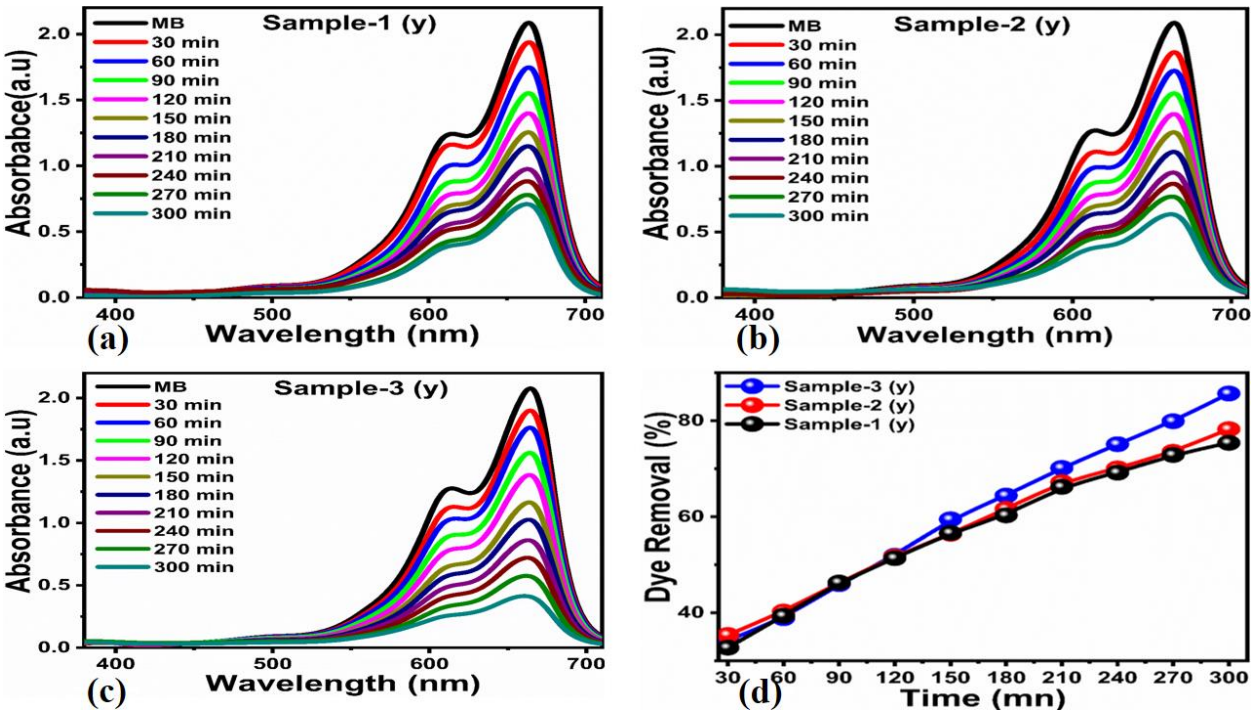

S15: UV-visible absorbance spectra in MB concentration of 3.4 $\times 10^{-5}$ M for the time interval of 300 min under the illumination of natural sunlight (a) 5 mg catalyst dose ZnO immobilized onto 1 gram of DSS, (b) 10 mg catalyst dose ZnO immobilized onto 2 gram of DSS, (c) 10 mg catalyst dose ZnO immobilized onto 4 gram of DSS, (d) Degradation efficiency of 10 mg catalyst dose ZnO immobilized onto 1, 2 and 4 grams of DSS

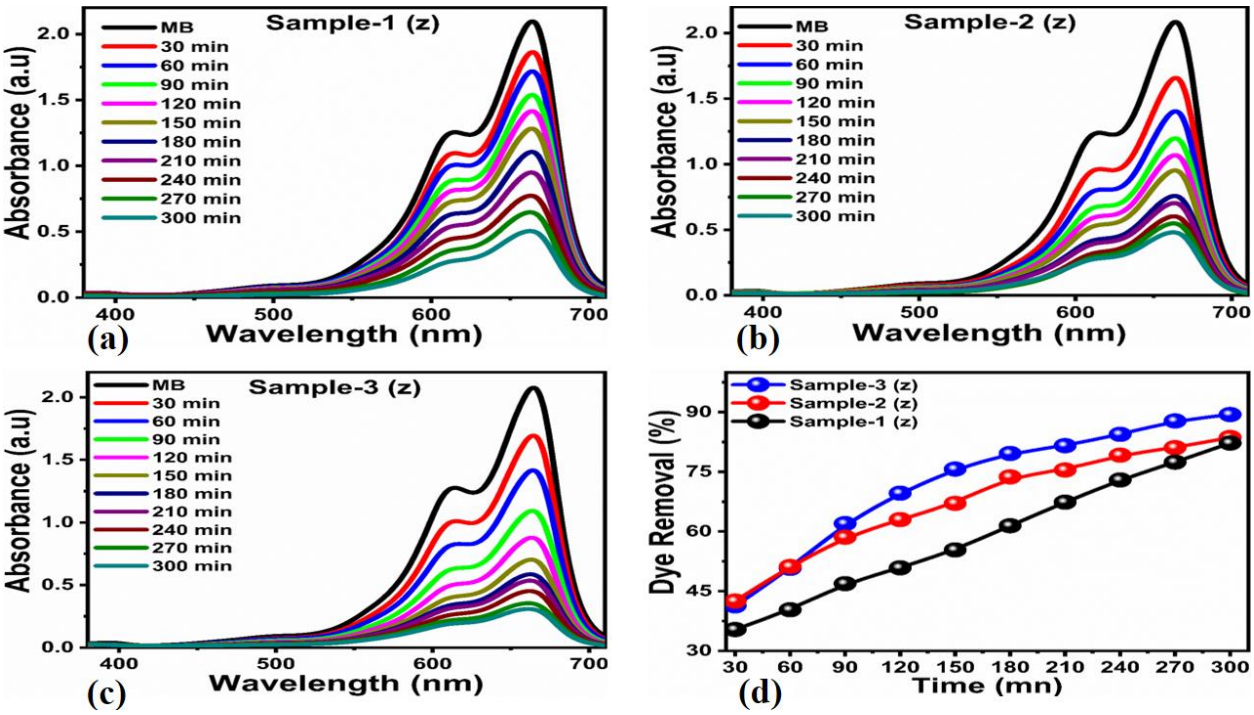

S16: UV-visible absorbance spectra in MB concentration of 3.4 $\times 10^{-5}$ M for the time interval of 300 min under the illumination of natural sunlight (a) 15 mg catalyst dose ZnO immobilized onto 1 gram of DSS, (b) 15 mg catalyst dose ZnO immobilized onto 2 gram of DSS, (c) 15 mg catalyst dose ZnO immobilized onto 4 gram of DSS, (d) Degradation efficiency of 15 mg catalyst dose ZnO immobilized onto 1, 2 and 4 grams of DSS

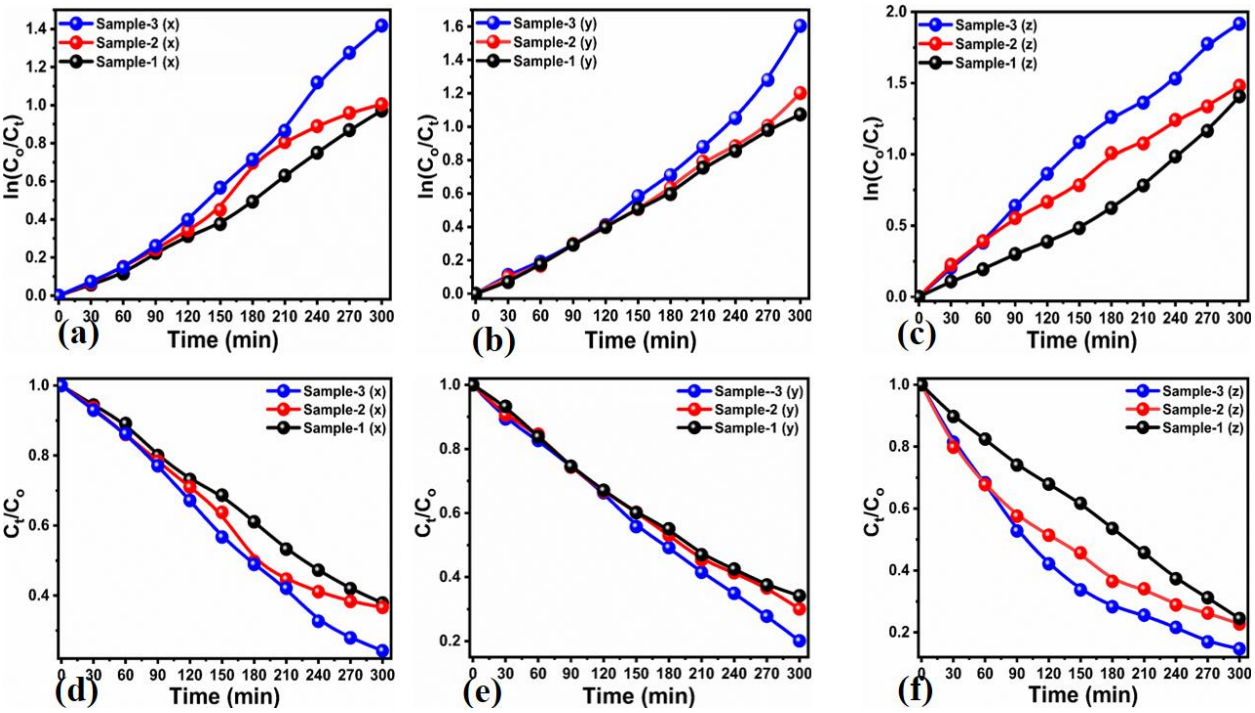

S17: Linear plotting for kinetic versus different time intervals in MB concentration of 3.4 ×10^{-5} M for the time interval of 300 min (a) 5 mg catalyst dose of ZnO immobilized onto 1, 2 and 4 grams of DSS, (b) 10 catalyst dose ZnO immobilized onto, 1, 2 and 4 grams of DSS, (c) 15 mg catalyst dose ZnO immobilized onto 1, 2 and 4 gram of DSS, (d) Photodegradation reaction profile for MB concentration of 3.4 ×10^{-5} M for the time interval of 300 min for 5 mg catalyst dose of ZnO immobilized onto 1, 2 and 4 grams of DSS, (e) 10 catalyst dose ZnO immobilized onto, 1, 2 and 4 grams of DSS, (f) 15 mg catalyst dose ZnO immobilized onto 1, 2 and 4 gram of DSS

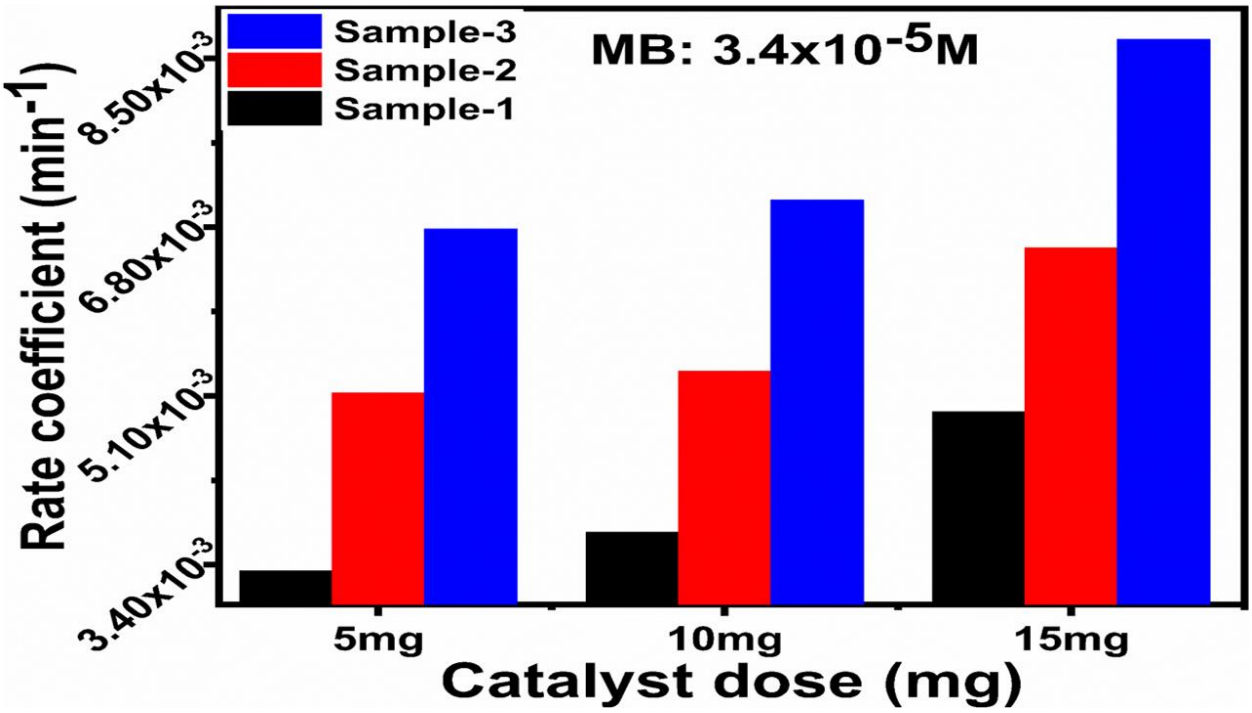

S 18: Pictorial presentation of rate constants for the 5, 10 and 15 mg catalyst dose of each ZnO immobilized onto 1, 2 and 4 grams of DSS in in MB concentration of 3.4 $\times 10^{-5}$ M for the time interval of 300 min.

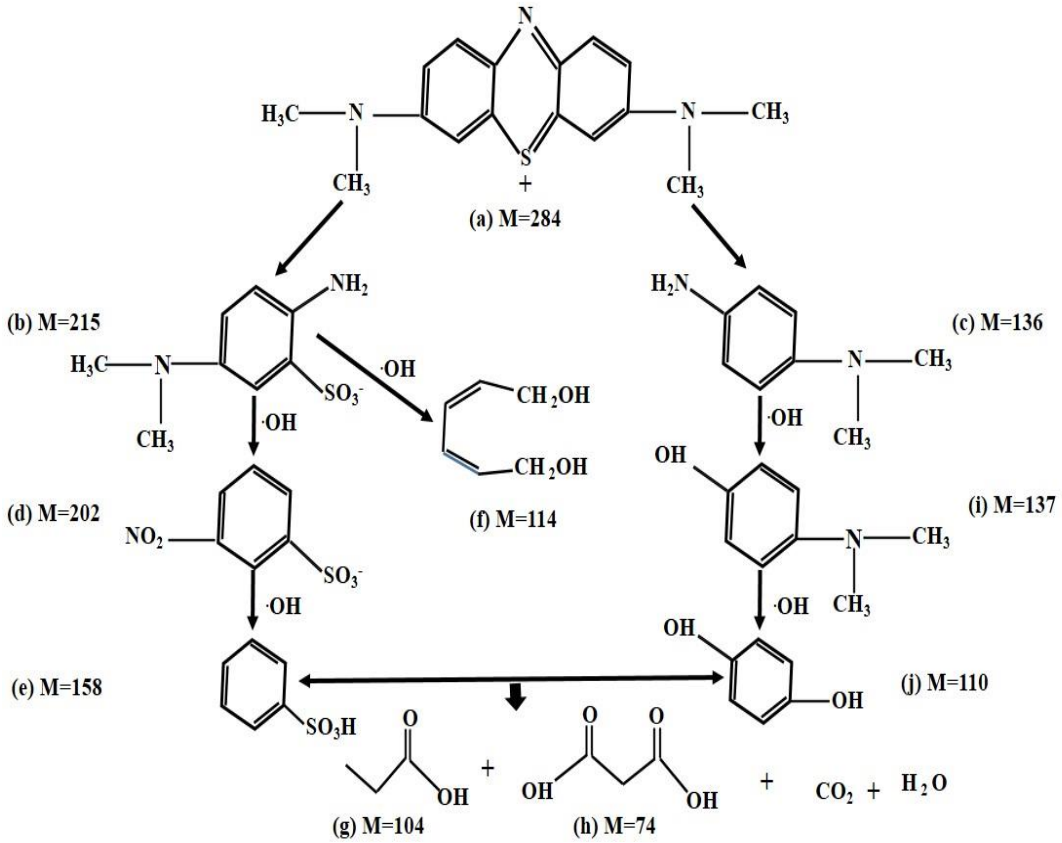

S19: Experimentally identified products during the degradation of MB in aqueous solution

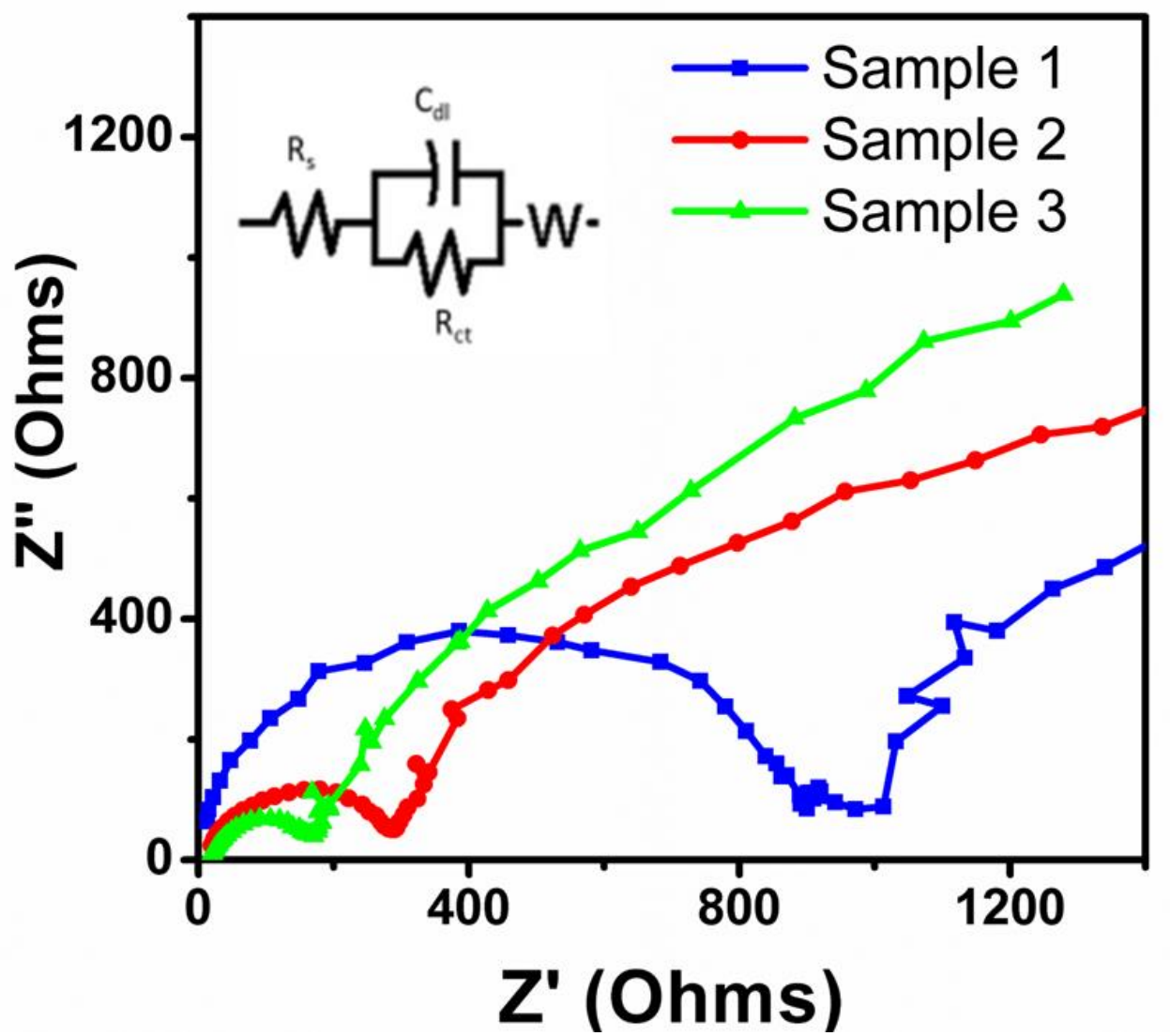

S20: EIS spectra of pure DSS (sample1), pristine ZnO (sample 2) and ZnO/DSS hybrid photocatalyst containing high amount of DSS (sample3)

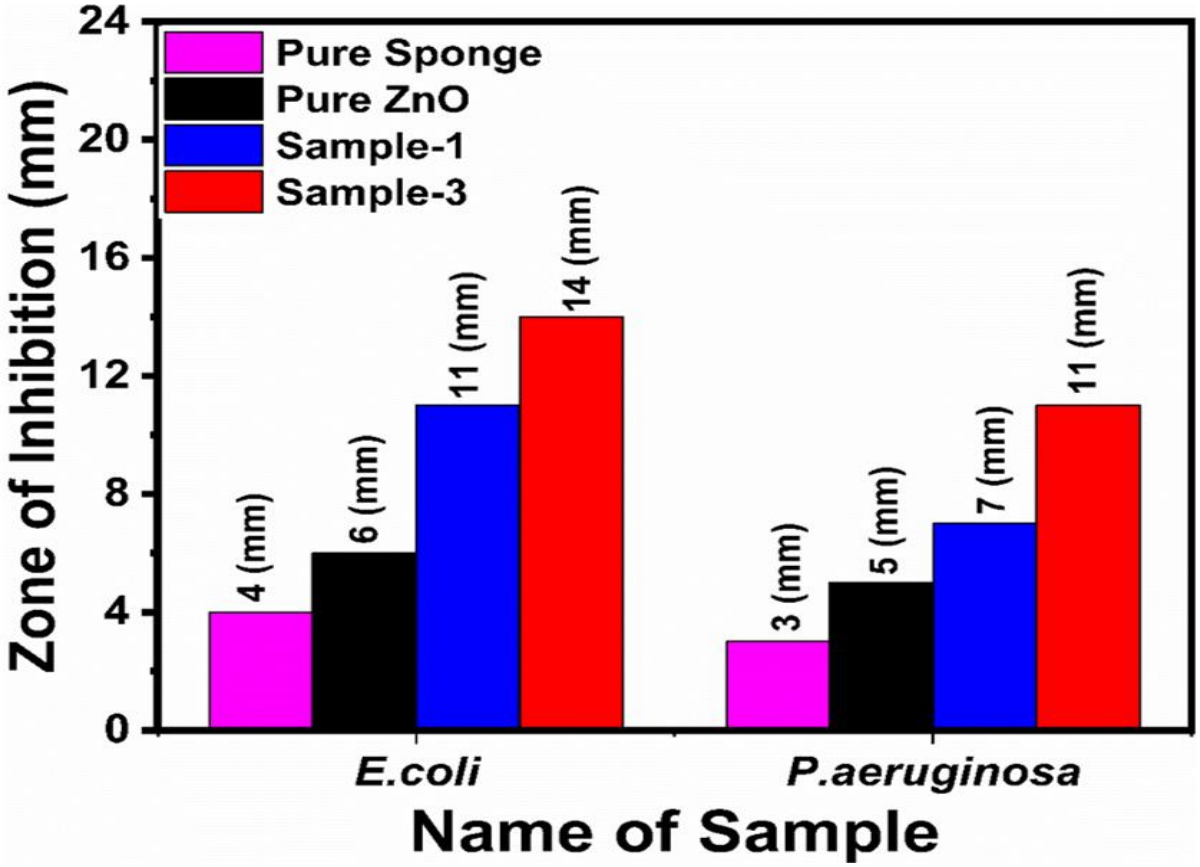

S21: Antibacterial study of pure ZnO and ZnO immobilized onto 1, 2 and 4 grams of DSS against *E.coli* and *P.aeruginosa*

Table S1: Recalculated rate constant for different regions of sample-3

Sample Name	K value (min^{-1}) Region-1	K value (min^{-1}) Region-2	Average K value (min^{-1})
Sample-3 (a)	0.008841	0.030775	0.019808
Sample-3 (b)	0.01277	0.03629	0.02453
Sample-3 (c)	0.012542	0.07243	0.042486

Table S2: The comparative analysis of 15 mg catalyst dose of ZnO immobilized onto 4 grams of DSS with various well-established photocatalysts

Catalysts	Weight	Light Source	Dye Con:	Time (min)	Dye Removal (%)	Method	Ref.
S-ZnO NPs	30mg	Sun light	MB 20 μM	45	61.45%	Co-precipitation	[1]
$MnTiO_3$	5mg	Sun light	MB $1 \times 10^{5-}$ M	250	75%	Sol-gel	[2]
CBMO	150mg	Sunlight	MB 1 g	120	67.43%	Co-precipitation	[3]
Fe_2TiO_5	50mg	Sunlight	MB 10 mg l^{-1}	250	97%	Sol-gel	[4]

PP–ZnONPs	50mg	Sunlight	MB 20 ppm	120	95%	GS-Method	[5]
3-BiOI/SiO_2	3g	Visible light LED lamp	MB 10 mg L^{-1}	15h	86.2%	One-pot solvothermal	[6]
ZnO Nps	100mg	Sunlight	MB 10ppm	150	91%	Combustion	[7]
porous TiO_2 ceramics	eighty pieces (20 mg each piece)	UV light	RhB 10 mg L^{-1}	300 min	99.3%	camphene-based freeze-casting process	[8]
macro/mesoporous anatase TiO_2 ceramic	eighty pieces (20 mg each piece)	UV light	RhB 10 mg mL^{-1}	180	99.4%	a camphene-based freeze-casting process	[9]
exfoliated vermiculite	2g	Sun light	phosphate	26h	50%	microwave irradiation to give EV a floating property	[10]
Fe–N-codoped TiO_2/fly ash cenospheres	0.2g	Sun light	RhB mg L^{-1}	4 h	89%	Sol-gel method	[11]
hollow TiO_2/fly ash cenospheres	1.5g	Sun light	MB 30 mg L^{-1}	9 h	0.0922 (min^{-1})	Sol-gel	[12]
Ag^+-doped TiO_2/polystyrene	0.05g	Sun light	MB 5 mg L^{-1}	5h	83%	Impregnation and strewing based on a simple solvent-cast method	[13]
TiO_2/polyurethane foam	forty pieces	Sun light	MB + Cr^{VI} 10 mg L^{-1}	150	90%	a low-temperature ultrasonic and deposition approach	[14]
TiO_2/low density polyethylene	1g	Sun light	MB 0.16 mmol L^{-1}	225	30%		[15]
C,N-TiO_2/polytetrafluoroethylene	1gL^{-2}	Visible light	MO 20 mg L^{-1}	4h	96.9%	y a simple high-energy ball-milling process	[16]

B–N–TiO_2/expanded perlite	(6 mg/g, 24 wt% TiO_2	Solar light	RhB	5h	99.1%	Sol-gel	[17]
Ag+-TiO2/PS	----	Solar light	MB 5 mg L−1	6h	94%	A simple solvent cost method	[18]
TiO_2-graphene	0.2 g	UV light	RhB 0.02 mM	2-4h	95%	Sol-gel	[19]
TiO_2/polypropylene	15–20 mg	UV light	MO 15 mg L^{-1}	4h	65%	Low temperature Hydrothermal method	[20]
TiO_2/polypropylene fabric	a piece (d = 47 mm)	UV light	MO 15 mg L^{-1}	240	100%	Hydrothermal Process	[21]
$MgAl_2O_4$-AC	0.1 g	Solar light	MB 30 mg/L	140	96%	Solvothermal	[22]
rGO/CuS	100 mg	Solar light	MG 10 mg/L	90	97.6	Co-precipitation method	[23]
ZnO–ZnTe	30mg	Solar light	MB 8 mg/L	2h	91%	one-pot hydrothermal approach	[24]
ZnO/ZnSe/$MoSe_2$	0.03 g	Solar Light	MO 30 mg/L	180	91.5%	Modified So-Gel Methods	[25]
ZnO/Cr_2O_3	25mg	Solar Light	MB 10 ppm	90	85%	Green method	[26]
ZnO/C-dots	20 mg	Solar Light	RO 5×10^{-5}M	8h	85%	one-step method.	[27]
Fe_3O_4/silica/ZnO	500mg	Solar light	MB 5 ppm)	60	99%	coprecipitation and solvothermal methods	[28]
Dy-doped ZnO	0.2g	Solar light	MB 1×10^{-5} M	75	97%	tartaric acid-assisted combustion method	[29]
ZnO/C	3 wt% carbon nanoplates	500 W Hg visible lamp	MB 25 mg/L	80	95%	wet chemical method	[30]
Mn–ZrO_2 NPs	20.0 mg	Solar light	MB 10.0 mg L^{-1}	60	96.2%	simple co-precipitation Method	[31]

Fe_3O_4/ZnO	0.2g	Solar Light	MB 100 ppm	120	85.5%	solid-state method	[32]
Ni–Th–ZnO	0.375 g/ L	Solar Light	MB 1.5 μM	180	93%	co-precipitation method	[33]
La-doped ZnO	10mg	Solar Light	5×10^{-5} M	100	85%	wet chemical method	[34]
Cd-doped ZnO	25mg	Soalr Light	MB 10 mg/L = 3.0×10^{-5} M	3.5h	85.0%	Sol-Gel Method	[35]
ZnO coated on 4g of DSS	15 mg	Solar Light	MB 2.50×10^{-5} M	160	99.94%	Simple Hydrothermal Process	Present Work

Table S3: Antibacterial assessment of ZnO and ZnO coated Sponge samples

Name of Sample	**Zone of inhibition (mm)**	
	E.coli	*P.aeruginosa*
Pure Sponge	4 mm	3 mm
Pure ZnO	6 mm	5 mm
Sample-1	11 mm	7 mm
Sample-3	14 mm	11 mm

References

[1]. Thambidurai S, Gowthaman P, Venkatachalam M and Suresh S 2020 Natural sunlight assisted photocatalytic degradation of methylene blue by spherical zinc oxide nanoparticles prepared by facile chemical co-precipitation method *Optik*, **207** 163865.

[2]. Alkaykh S, Mbarek A and Ali-Shattle EE 2020 Photocatalytic degradation of methylene blue dye in aqueous solution by MnTiO3 nanoparticles under sunlight irradiation *Heliyon*. ***6*** e03663.

[3]. Makeswari M and Saraswathi P 2020 Photo catalytic degradation of methylene blue and methyl orange from aqueous solution using solar light onto chitosan bi-metal oxide composite *SN Applied Sciences **2*** pp.1-12.

[4]. Vasiljevic ZZ, Dojcinovic MP, Vujancevic JD, Jankovic-Castvan I, Ognjanovic M, Tadic NB, Stojadinovic , Brankovic GO and Nikolic MV 2020 Photocatalytic degradation of methylene blue under natural sunlight using iron titanate nanoparticles prepared by a modified sol–gel method *Royal Society open science*. **7** 200708.

[5]. Pai S, Sridevi H, Varadavenkatesan T, Vinayagam R and Selvaraj R 2019 Photocatalytic zinc oxide nanoparticles synthesis using Peltophorum pterocarpum leaf extract and their characterization *Optik*. **185** 248-255.

[6]. Qiu H, Zhang R, Yu Y, Shen R and Gao H 2020 BiOI-on-SiO2 microspheres: A floating photocatalyst for degradation of diesel oil and dye wastewater *Science of the Total Environment*. **706** 136043.

[7]. Nagaraju G, Shivaraju GC, Banuprakash G and Rangappa D 2017 Photocatalytic activity of ZnO nanoparticles: synthesis via solution combustion method *Materials Today: Proceedings*. ***4*** 11700-11705.

[8]. Xing Z, Li J, Wang Q, Zhou W, Tian G, Pan K, Tian C, Zou J and Fu H 2013 A floating porous crystalline TiO2 ceramic with enhanced photocatalytic performance for wastewater decontamination *European Journal of Inorganic Chemistry*. **13** 2411-2417.

[9]. Xing Z, Zhou W, Du F, Qu Y, Tian G, Pan K, Tian C and Fu H 2014 A floating macro/mesoporous crystalline anatase TiO 2 ceramic with enhanced photocatalytic performance for recalcitrant wastewater degradation *Dalton Transactions*. ***43*** 90-798

[10]. Lee T, Lee S, Lee J and Lim JH 2016 Modification of vermiculite for the preparation of floating adsorbent for phosphate in wastewater *Water Environment Research*. ***88*** 724-731.

[11]. Song J, Wang X, Bu Y, Zhang J, Wang X, Huang J, Chen J and Zhao J 2016 Preparation, characterization, and photocatalytic activity evaluation of Fe–N-codoped TiO 2/fly ash cenospheres floating photocatalyst. *Environmental Science and Pollution Research*, ***23*** 22793-22802.

[12]. Wang B, Li C, Pang J, Qing X, Zhai J and Li Q 2012 Novel polypyrrole-sensitized hollow TiO2/fly ash cenospheres: Synthesis, characterization, and photocatalytic ability under visible light *Applied Surface Science*. ***258*** 9989-9996.

[13]. Singh S, Singh PK and Mahalingam H 2014 Novel floating Ag+-doped TiO2/polystyrene photocatalysts for the treatment of dye wastewater *Industrial & Engineering Chemistry Research*. ***53*** 16332-16340.

[14]. Zhang L, Xing Z, Zhang H, Li Z, Zhang X, Zhang Y, Li L and Zhou W Multifunctional floating titania-coated macro/mesoporous photocatalyst for efficient contaminant removal *ChemPlusChem*. ***80*** 623.

[15]. Magalhães F, Moura FC and Lago RM 2011TiO2/LDPE composites: A new floating photocatalyst for solar degradation of organic contaminants *Desalination*. ***276*** 266-271.

[16]. Zhong W, Yu Y, Du C, Li W, Wang Y, He G, Xie Y and He Q 2011 Characterization and high pollutant removal ability of buoyant (C, N)–TiO 2/PTFE flakes prepared by high-energy ball-milling *RSC Advances*. ***4*** 40019-40028

[17]. Xue H, Jiang Y, Yuan K, Yang T, Hou J, Cao C, Feng K and Wang X 2016 Floating photocatalyst of B–N–TiO 2/expanded perlite: a sol–gel synthesis with optimized mesoporous and high photocatalytic activity. *Scientific reports*, *6*(1), (2016), pp.1-9.

[18]. Singh S, Singh PK and Mahalingam H 2014 Novel floating Ag+-doped TiO2/polystyrene photocatalysts for the treatment of dye wastewater. *Industrial & Engineering Chemistry Research*. ***53*** 16332-16340

[19]. Modestov A, Glezer V, Marjasin I, Lev O 1997Photocatalytic degradation of chlorinated phenoxyacetic acids by a new buoyant titania-exfoliated graphite composite photocatalyst *The Journal of Physical Chemistry B*. **101** 4623-4629

[20]. Han H and Bai R 2009 Buoyant photocatalyst with greatly enhanced visible-light activity prepared through a low temperature hydrothermal method *Industrial & Engineering Chemistry Research*. ***48*** 2891-2898.

[21]. Han H and Bai R 2010 Highly effective buoyant photocatalyst prepared with a novel layered-TiO2 configuration on polypropylene fabric and the degradation performance for

methyl orange dye under UV–Vis and Vis lights *Separation and Purification Technology*. **73** 142-150.

[22]. Asl EA, Haghighi M and Talati A 2020 Enhanced simulated sunlight-driven magnetic MgAl2O4-AC nanophotocatalyst for efficient degradation of organic dyes *Separation and Purification Technology*. **251** 117003.

[23]. El-Hout SI, El-Sheikh SM, Gaber A, Shawky A and Ahmed AI 2020 Highly efficient sunlight-driven photocatalytic degradation of malachite green dye over reduced graphene oxide-supported CuS nanoparticles *Journal of Alloys and Compounds*. **849** 156573.

[24]. Raza N, Raza W, Gul H and Kim KH 2021 ZnO–ZnTe hierarchical superstructures as solar-light-activated photocatalysts for azo dye removal *Environmental research*. **194** 110499

[25]. Yang Y, Wu Z, Yang R, Li Y, Liu X, Zhang L and Yu B 2021 Insights into the mechanism of enhanced photocatalytic dye degradation and antibacterial activity over ternary ZnO/ZnSe/MoSe2 photocatalysts under visible light irradiation *Applied Surface Science*. **539** 148220.

[26]. Zelekew OA, Fufa PA, Sabir FK and Duma AD 2021 Water hyacinth plant extract mediated green synthesis of Cr2O3/ZnO composite photocatalyst for the degradation of organic dye *Heliyon*. e07652.

[27]. Kalaiarasan S, Uthirakumar P, Shin DY and Lee IH 2021 The degradation profile of high molecular weight textile reactive dyes: A daylight induced photocatalytic activity of ZnO/carbon quantum dot photocatalyst *Environmental Nanotechnology, Monitoring & Management*. **15** 100423.

[28]. Atla SB, Lin WR, Chien TC, Tseng MJ, Shu JC, Chen CC and Chen CY 2018 Fabrication of Fe3O4/ZnO magnetite core shell and its application in photocatalysis using sunlight *Materials Chemistry and Physics*. **216** 380-386

[29]. Sa-nguanprang S, Phuruangrat A, Thongtem T and Thongtem S 2020 Characterization and photocatalysis of visible-light-driven Dy-doped ZnO nanoparticles synthesized by

tartaric acid-assisted combustion method *Inorganic Chemistry Communications*. **117** 107944.

[30]. Micheal K, Ayeshamariam A, Devanesan S, Bhuvaneswari K, Pazhanivel T, AlSalhi MS, Aljaafreh MJ 2020 Environmental friendly synthesis of carbon nanoplates supported ZnO nanorods for enhanced degradation of dyes and organic pollutants with visible light driven photocatalytic performance *Journal of King Saud University-Science*. **32** 1081-1087.

[31]. Ahmed W and qbal J 2021 Mn doped ZrO2 nanoparticles: An optically tuned photocatalyst with superior structural, magnetic and dielectric characteristics. *Journal of Physics and Chemistry of Solids*. 110285.

[32]. Elshypany R, Selim H, Zakaria K, Moustafa AH, Sadeek SA, Shara SI, Raynaud P and Nada AA 2021 Elaboration of Fe3O4/ZnO nanocomposite with highly performance photocatalytic activity for degradation methylene blue under visible light irradiation *Environmental Technology & Innovation*. 101710.

[33]. Vignesh K, Rajarajan M and Suganthi A 2014 Visible light assisted photocatalytic performance of Ni and Th co-doped ZnO nanoparticles for the degradation of methylene blue dye *Journal of Industrial and Engineering Chemistry*. **20** 3826-3833.

[34]. Bomila R, Srinivasan S, Gunasekaran S, Manikandan A 2018 Enhanced photocatalytic degradation of methylene blue dye, opto-magnetic and antibacterial behaviour of pure and La-doped ZnO nanoparticles *Journal of Superconductivity and Novel Magnetism*. **31** 855-864.

[35]. Zhang D and Zeng F 2012 Visible light-activated cadmium-doped ZnO nanostructured photocatalyst for the treatment of methylene blue dye *Journal of Materials Science*. **47** 2155-2161.